Neurobiology of Disease 132 (2019) 104560

Contents lists available at ScienceDirect

Neurobiology of Disease

journal homepage: www.elsevier.com/locate/ynbdi

Leptin deficiency reverses high metabolic state and weight loss without affecting central pathology in the R6/2 mouse model of Huntington's disease

Marie Sjögren[a,*], Rana Soylu-Kucharz[a], Unali Dandunna[a], Tiberiu Loredan Stan[a], Michele Cavalera[b], Åsa Sandelius[c], Henrik Zetterberg[c,d,e,f], Maria Björkqvist[a]

[a] Wallenberg Neuroscience Center, Brain Disease Biomarker Unit, Department of Experimental Medical Sciences, Lund University, Lund, Sweden
[b] Department of Clinical Sciences, Cardiovascular Research, Translational Studies, Lund University, Malmö, Sweden
[c] Institute of Neuroscience and Physiology, Department of Psychiatry and Neurochemistry, The Sahlgrenska Academy at University of Gothenburg, Mölndal, Sweden
[d] Clinical Neurochemistry Laboratory, Sahlgrenska University Hospital, Mölndal, Sweden
[e] Department of Neurodegenerative Disease, UCL Institute of Neurology, London, United Kingdom
[f] UK Dementia Research Institute at UCL, London, United Kingdom

ARTICLE INFO

Keywords:
Leptin-deficiency
Energy metabolism
Oxygen consumption
Adipose tissue
Huntington's disease

ABSTRACT

Body weight has been shown to be a predictor of clinical progression in Huntington's disease (HD). Alongside widespread neuronal pathology, both HD patients and the R6/2 mouse model of HD exhibit weight loss and increased energy expenditure, providing a rationale for targeting whole-body energy metabolism in HD. Leptin-deficient mice display low energy expenditure and increased body weight. We therefore hypothesized that normalizing energy metabolism in R6/2 mice, utilizing leptin- deficiency, would lead to a slower disease progression in the R6/2 mouse.

In this study, we show that R6/2 mice on a leptin-deficient genetic background display increased body weight and increased fat mass compared to R6/2 mice, as well as wild type littermates. The increased body weight was accompanied by low energy expenditure, illustrated by a reduction in respiratory exchange rate. Leptin-deficient R6/2 mice had large white adipocytes with white adipocyte gene expression characteristics, in contrast to white adipose tissue in R6/2 mice, where white adipose tissue showed signs of browning. Leptin-deficient R6/2 mice did not exhibit improved neuropathological measures.

Our results indicate that lowering energy metabolism in HD, by increasing fat mass and reducing respiratory exchange rate, is not sufficient to affect neuropathology. Further studies targeting energy metabolism in HD are warranted.

1. Introduction

Huntington's disease (HD) is associated with progressive motor, cognitive and functional decline (Novak and Tabrizi, 2010; Walker, 2007), symptoms that are caused by an expanded CAG trinucleotide repeat in HTT, the gene encoding the protein huntingtin (Group, 1993; Ross and Tabrizi, 2011; Sathasivam et al., 1999). The mutation causes the protein to gain toxic functions and aggregate, resulting in neuronal dysfunction and death (Bates et al., 2015; Ross and Tabrizi, 2011). Although substantial progress has been made in understanding mechanisms underlying HD pathology, this is not fully understood.

Accumulating evidence suggests altered energy metabolism and a hyper-catabolic state as key features of HD pathology (Carroll et al., 2015; van der Burg et al., 2009, 2011). Body weight has been shown to be a predictor of clinical HD progression and higher BMI is demonstrated to be associated with a slower rate of functional, cognitive and motor decline (van der Burg et al., 2017). Studies have investigated the potential therapeutic impact of dietary manipulations in HD and report various beneficial effects (Andreassen et al., 2001; Dedeoglu et al., 2003; Mochel et al., 2010). However, it is not known whether dietary manipulations alter the hypermetabolic state in HD.

The R6/2 mouse model of HD mirrors human HD and in addition to central pathological changes (Bates et al., 2015), the mice exhibit progressive weight loss (van der Burg et al., 2008, 2011), altered body composition (She et al., 2011) and increased oxygen consumption (Goodman et al., 2008; Li et al., 2005; van der Burg et al., 2008). Hyperplasia of brown/beige cells in white adipose tissue (WAT) has been shown to enhance energy expenditure (Bartelt and Heeren, 2014) and browning of R6/2 mouse WAT has been shown to be linked to increased energy metabolism, possibly contributing to HD weight loss (McCourt

* Corresponding author at: Wallenberg Neuroscience Center EMV, BMCA10, Lund University, 22184 Lund, Sweden.
E-mail address: marie.sjogren@med.lu.se (M. Sjögren).

https://doi.org/10.1016/j.nbd.2019.104560
Received 17 February 2019; Received in revised form 13 June 2019; Accepted 30 July 2019
Available online 13 August 2019
0969-9961/

et al., 2016).

In amyotrophic lateral sclerosis (ALS), an association between high energy metabolism and clinical progression has been demonstrated (Dupuis et al., 2011) and different ways to change metabolic state have been investigated as disease modification strategies (Coughlan et al., 2016; Lim et al., 2014; Park et al., 2007). Leptin (encoded by the *ob* gene) is an adipokine that plays a central role in energy homeostasis, appetite and weight regulation (Maffei et al., 1995). Ob/Ob mice are leptin-deficient; they exhibit increased food intake and have a slower energy metabolism leading to increased body weight, linked to increased fat mass (Garthwaite et al., 1980; Ingalls et al., 1996; Mayer et al., 1953). Notably, ALS mice on a leptin-deficient genetic background have been shown to have normalized energy expenditure, improved motor function, decreased motor neuronal loss, as well as enhanced survival, suggesting a slower rate of the disease progression (Lim et al., 2014).

In this study, we therefore aimed to investigate whether an altered energy metabolism and increased body weight can affect R6/2 mouse disease measures. We used a genetic approach and crossed the R6/2 mouse with leptin-deficient Ob/Ob mice and investigated central and peripheral parameters as well as behaviour and energy metabolism measures.

We can here demonstrate that it is possible to dramatically increase R6/2 mouse body weight by changing energy metabolism, however this is not associated with improved neuropathological measures.

2. Materials and methods

2.1. Ethics

Animal experiments were carried out in strict accordance with Swedish legislation and approved by local and national regulatory authorities (permit number: 2505/2018), (Animal Ethics Committee in Lund and Malmö, Sweden).

2.2. Animals

A two-step breeding strategy was used to generate leptin-deficient R6/2 mice (R6/2;Ob/Ob) (see Supplementary Fig. 1). Females heterozygous for the obese gene (Ob−/+) on the C57BL/6J genetic background (Strain #000632, Jackson Laboratory, Bar Harbor, ME, USA) were crossed with males heterozygote for the R6/2 gene on the C57BL/6xCBA genetic background (Jackson Laboratory, Bar Harbor, ME, USA). Mutant R6/2;Ob−/+ males from the F1 generation were crossed with Ob−/+ females to generate the F2 generation, containing WT, R6/2, Ob−/+, Ob/Ob, R6/2;Ob−/+ and R6/2;Ob/Ob littermates. R6/2 mice with the mutant leptin heterozygote and homozygote genetic backgrounds are denoted as R6/2;Ob−/+ and R6/2;Ob/Ob, respectively. Non-transgenic mice are denoted as wild type (WT), Ob−/+ (mutant leptin heterozygote) and Ob/Ob (mutant leptin homozygote) (Supplementary Fig. 1). Generated genotype frequencies for generation 1 was 25% for each genotype, while for generation 2, the generated genotype frequency was 25% for Ob−/+ and R6/2;Ob−/+ and 12.5% for WT, R6/2, R6/2;Ob/Ob and Ob/Ob. For genotyping, ear punch samples were taken at 4 weeks of age and genotyped for the R6/2 and Ob gene using PCR. The PCR product (Ob) was cleaved with HpyF3I restriction enzyme (Thermo Scientific, Rockford, IL, USA). PCR products were separated by gel electrophoresis using a 3% agarose gel for detecting the Ob gene, and 2% for the R6/2 gene. All primers were purchased from MWG Eurofins (Eurofins MWG Synthesis GmbH, Germany), and sequences of all primers used for genotyping in this study are found in Supplementary Table 1. Tail tips were sent to Laragen (Laragen Inc., CA, USA) for CAG repeat length determination. The CAG-repeat lengths of the R6/2, R6/2;Ob−/+ and R6/2;Ob/Ob mice from two different strains used in this study ranged either between 345 and 352 or 242–257. The CAG repeat size of our colony, results in a disease progression slower than that of the R6/2 mouse with 150 CAG repeats, as described by Morton and co-workers in 2009 (Morton et al., 2009).

The mice were housed in groups of 2–5 in universal Innocage mouse cages (InnoVive, San Diego, CA, USA) under standard conditions (12 h light/dark cycle, 22 °C), and with ad libitum access to chow food, water and cages were enriched with nesting material.

At end-point, after an eight hour fast, the mice anesthetized with pentobarbital (Apoteksbolaget, Lund, Sweden) during blood collection, and then euthanized and tissue samples; brain (cortex, striatum), intra-abdominal epididymal white adipose tissue (WAT), interscapular brown adipose tissue (BAT), skeletal muscle (gastrocnemius), were dissected and snap-frozen in liquid nitrogen and stored at −80 °C until further use.

Blood samples were collected at the time of sacrifice, from the right heart ventricle using a wide-bore needle (18 G/40 mm), to prevent applying large suction force. Blood samples were stored at room temperature for 30 min and then centrifuged at ~2500 ×*g* for 15 min to obtain serum.

Cerebrospinal fluid (CSF) samples were collected from 4th ventricles under terminal dose of pentobarbital anesthesia. The heads of the mice were mounted on a stereotaxic frame, and the skin and muscle tissue were dissected to expose the dura mater above the cisterna magna. CSF samples were collected using glass capillaries (outer diameter = 80 μm) connected to 1 ml syringe through polyethylene tubing. CSF and serum were snap-frozen in liquid nitrogen and stored at −80 °C until further use.

2.3. Serum, blood and tissue analyses

Fasting serum and cortical homogenate leptin levels were measured using the Mouse Leptin ELISA kit (Crystal Chem, Zaandam, Netherlands), with a detection range of 0.2–12.8 ng/ml. Samples were assessed in duplicates according to manufacturer's protocol.

Fasting serum glucose levels were measured using the glucose oxidase method (Thermo Trace, Victoria, Australia), and levels of insulin were determined by radioimmunoassay (RIA; Linco Research Inc., St. Louis, MO, USA), both according to manufacturer's protocols and samples assessed in duplicates. The homeostatic model assessment (HOMA), a method widely used to assess insulin resistance (IR) and pancreatic beta-cell function (β) from fasting glucose and insulin or C-peptide concentrations, was first described by Matthews et al., 1985. HOMA-IR was calculated as follows: (Insulin X Glucose)/22.5, and HOMA-β as follows: (20 X Insulin)/(Glucose-3.5) (Matthews et al., 1985; Wallace et al., 2004).

Fasting serum total, HDL and LDL/VLDL cholesterol levels were measured using HDL and LDL/VLDL Quantification Colorimetric/Fluorometric Kit (BioVision, Milpitas, CA, USA) according to manufacturer's protocol and samples assessed in duplicates. The ratio between LDL/VLDL and HDL was calculated.

2.4. Body weight and composition measurements

Body weight was assessed twice a week from the age of 6 weeks. Body composition (fat and lean mass) was measured using the Lunar Prodigy dual-energy x-ray absorptiometry (DEXA; GE Lunar Corp., Madison, WI) in isoflurane-anesthetized (Apoteksbolaget, Lund, Sweden) mice.

2.5. Indirect gas calorimetry

The animals were habituated to the drinking bottles one-day prior acclimatization. Whole-body energy metabolism, locomotor activity, and food and water intake were measured using the PhenoMaster Home Cage System (TSE-systems, Bad Homburg, Germany). Animals were weighed, single-housed and acclimatized to the calorimeter chambers

for one day prior to the experiments. Food and water were available ad libitum. All parameters were recorded every 15 min for 24 h, and reported as light phase, dark phase and 24 h. Metabolic rates were calculated using a correction for body weight.

2.6. Adipose tissue histology

Intra-abdominal epididymal white (WAT) and interscapular brown (BAT) adipose tissue from males at 20 weeks were dissected, placed into 4% paraformaldehyde in phosphate buffered saline (0.01 M) overnight. Tissues were then transferred to 70% ethanol solution and stored at 4 °C before paraffin embedding. Sections (7 μm) were mounted on glass slides and stained according to Mayer's Hematoxylin-Eosin staining protocol. Digital images of the stained sections were used to identify the morphological features of WAT and BAT, and adipocytes (> 150 cells) of WAT from each mouse were selected for area measurements at 20× magnification. Cell areas were measured using cellSens Dimensions 1.11 software (Olympus U-HSCBM, Olympus, Tokyo, Japan). Slides were coded, and the operator was unaware of the genotype of each sample during analyses for blinded measuring. Mean adipocyte (WAT) areas for each group were then compared. A bright-light microscope (Olympus U-HSCBM, Olympus, Tokyo, Japan) with a 20× magnification objective, digital camera and image capture software (cellSens Dimensions 1.11 software; Olympus, Tokyo, Japan) were used.

2.7. CSF analyses

CSF neurofilament light chain (NfL) concentration was assessed as previously described using the in-house Simoa NfL assay (Rohrer et al., 2016). The repeatability of two quality control samples was 6.8 CV% (coefficient of variation) for a sample with a mean NfL concentration of 87.2 pg/ml, and 4.7 CV% for a sample with a mean NfL concentration of 11.3 pg/ml. Determination of the lower limit of quantification has been described previously (Soylu-Kucharz et al., 2017).

2.8. Immunohistochemistry

Mice were perfused transcardially under terminal sodium pentobarbital anesthesia (Apoteksbolaget, Lund, Sweden) with saline and subsequently with ice-cold 4% paraformaldehyde (PFA) for 10 min (at the rate of 10 ml/min). Brains were extracted and placed in 4% PFA solution for 24 h at 4 °C for post-fixation, then transferred to 30% sucrose solution complemented with sodium azide at 4 °C until use. Brains were sectioned in the coronal plane (30 μm sections, six series per animal) on dry ice and the sections were stored at −20 °C in an antifreeze solution (30% glycerol, 30% ethylene glycol in phosphate buffer). Free-floating brain sections were rinsed with 0.01 M phosphate buffered saline (PBS) 3 times for 10 min. Next, the sections were incubated in 0.01 M citrate buffer, pH 8.5 at 80 °C for 40 min for the antigen retrieval. Sections were left in PBS containing 3% H_2O_2 and 10% methanol for quenching. The sections were pre-incubated for 1 h at room temperature (RT) with blocking solution containing 5% normal donkey serum and 1% bovine serum albumin (BSA) in 0.3% Triton X/PBS, followed by incubation with primary antibody (EM48 Millipore MAP 5374; mouse 1:400 dilution, EMD Millipore, Burlington, MA, USA) in blocking solution overnight on a shaker at 4 °C. The sections were washed 3 times for 10 min in PBS then incubated with secondary (biotinylated horse anti-mouse; 1:200 dilutions) antibody. Sections were rinsed with PBS and incubated with the avidin-biotin-peroxidase complex solution (VECASTAIN ABC Kit; Elite PK 6100 – Standard, Vector Laboratories Inc., Burlingame, CA USA) for 1 h at RT. The sections were rinsed with PBS 3x10min and then lastly incubated with 3′3 – Diaminobenidine (DAB) and H_2O_2 (DAB Kit SK-4100, Vector Laboratories Inc., Burlingame, CA USA) to visualize the aggregates. Finally, the sections are mounted on gelatine covered slides, dried overnight and dehydrated through a graded alcohol series to xylene and coverslipped with DPX mountant (Sigma Aldrich, Saint Louis, MO, USA).

For the assessment of striatal volume, cortex and corpus callosum thickness, cresyl violet (Nissl) staining was performed. First, free-floating brain sections were rinsed 3 times for 10 min with TBS to remove the antifreeze solution. The brain sections were mounted on gelatin-coated glass slides and air-dried at room temperature. The slides were passed through xylene and a series of decreasing ethanol solutions for 1 min each (100%, 95%, 70% ethanol). After dehydrating in distilled water for 1 min, the sections were left in 0.5% cresyl violet solution for 30 s to 1 min. The sections were dehydrated in increasing ethanol solutions (70%, 95%, 100%) and cleared in xylene for 5 min. Lastly, the glass slides were covered using DPX (Sigma-Aldrich, Saint Louis, MO, USA).

2.9. Stereological assessment

The experiments were carried out under the blinded conditions to genotypes. The volume of striatum, cortex and corpus callosum thickness were assessed on cresyl violet stained coronal sections in a blinded manner to genotypes. First, the cresyl violet strained brain sections were scanned using an automated digital microscope (Zeiss, Axio Zoom.V16). Next, using Zeiss Zen (Blue edition) software, dorsal striatum volume (bregma 1.70 mm to 0.38 mm), medial corpus callosum thickness (bregma 1.10 mm to 0.38 mm), and primary motor area Bregma (1.70 mm to 0.14. mm) were measured (Franklin and Paxinos, 2008).

Quantification for mHTT inclusions in the striatum and cortex were implemented on brain sections stained for EM48 antibody using DAB immunohistochemistry. Using Leica 20× objective (Leica, Germany) a series of z-stacks were collected. For the quantification of striatal inclusions, a total of 16 z-stack images collected per animal (4 *Z*-stack images from 4 consecutive brain sections between the bregma levels of anterior-posterior: 1.10 mm to 0.38 mm). The cortical inclusion quantifications were performed on the insular cortex and the sampling was performed between the bregma levels of anterior-posterior: 1.54 mm to 0.62 mm and 4 z-stack images were collected per animal (1 z-stack image from 4 consecutive sections of insular cortex). The z-stack images were processed using ImageJ/FijiJ (National Institutes of Health,

USA). Z-stack images were processed into two Z-projections; one with minimum intensity (converted to a reversed image) and the other with standard deviation. The two projections were processed into one image for analysis (Image Calculator) and the threshold was adjusted to automatic processing. The images were then analysed by particle size (pixel size minimum of 4 to infinity, though unspecific signals [i.e. dirt or small blood vessels] were manually excluded, and circularity of 0–1.0).

2.10. RNA extraction and cDNA synthesis

Total RNA was extracted from skeletal muscle gastrocnemius and white adipose tissue, using the E.Z.N.A. Total RNA Kit II (Omega biotek, Norcross, GA, USA) before complementary DNA (cDNA) was synthesized using iScript cDNA Synthesis Kit (Bio-Rad Laboratories, CA, USA), according to manufacturer's protocol. RNA concentration and purity were measured by a NanoDrop Lite spectrophotometer (Thermo Fisher Scientific, Wilmington, DE, USA).

2.11. Real-time quantitative PCR

SsoAdvanced Universal SYBR Green Supermix from Bio-Rad Laboratories was used for RT-qPCR and performed following manufacturer's protocol. All RT-qPCR plates were run on a CFX96 touch real-time PCR detection system (Bio-Rad, Hercules, CA, USA). Primers utilized for RT-qPCR validations were designed using either QuantPrime69 or PrimerQuest from Integrated DNA Technologies

(http://eu.idtdna.com/PrimerQuest). The efficiency of each primer pair was tested before use by performing a standard curve, and the efficiency criteria for using a primer pair was 90% < E < 110%, with an R^2 cut-off > 0.990. Housekeeping genes, Peptidylprolyl isomerase A (*Ppia*) and TATA Box Binding Protein (*Tbp*) were used for normalization of white adipose tissue (WAT) RT-qPCR, β-actin *(actb)* and ATP synthase, H+ transporting mitochondrial F1 complex, beta subunit *(Atp5b)* were used for normalization of striatal tissue RT-qPCR, and *Tbp* and 18S ribosomal RNA *(18S)* were used for normalization of skeletal muscle (gastrocnemius) RT-qPCR (Supplementary Table 2). Changes in gene expression were calculated using the CFX manager software program (Bio-Rad, Hercules, CA, USA), using the ΔΔCt method with a fold change cut-off at ≥1.5 and $p < .05$ considered significant. All samples were run in triplicate and relevant positive and negative controls were run on each plate.

2.12. Behavioural testing

Mice were handled prior to testing. Mice were transported in their home cages to the behavioural testing room and were allowed to acclimate to the room for at least one hour before testing.

2.12.1. Open field testing

Open field behaviour testing is a common measure of general activity and exploratory behaviour in rodents (Gould and Kovacsics, 2009), which has been shown to be affected in the HD mouse model R6/2 (Hickey et al., 2005). Motor activity (distance travelled) was evaluated in an additional group of mice in males at 19 weeks and females at 18 weeks during dark cycle in an open field arena with non-transparent open-topped Plexiglas boxes of 50 × 50 cm, using the Stoelting ANY-MAZE video tracking system (Dublin, Ireland), detecting position of the animal's head, body and tail. Mice were placed individually in the corner of the open field arena and were recorded for a 60-min period. Data was collected for every 5 min.

2.12.2. Nest building testing

Nest building is a natural and complex behaviour of mice, requiring fine motoric skills for pulling, carrying, and bedding of nest material, as well as the cognitive function for planning and problem solving, and an easy way of monitoring disease progression in neurodegenerative diseases (Deacon, 2006a, 2012). Nesting ability has been shown to be negatively affected in neurodegenerative diseases such as Alzheimer's disease (Deacon et al., 2008), Parkinson's disease (Paumier et al., 2013) and Huntington's disease (Sjögren et al., 2017). Nest building behaviour was assessed in males at 19 weeks and in females at 18 weeks. Mice were single caged overnight, with access to food and water, but with no environmental enrichment. Approximately 1.5 g of nesting material was placed in the cage, and torn material was weighed the next morning. Nesting ability was assessed on a point scale as previously described (Deacon, 2006a), from 1 to 5, analyzing both touched nesting material and shape of the nest. A score 1 was given when the nestlet was mainly untouched (> 90% was intact), score 3 was given when the nestlet was mostly shredded but no identifiable nest site was seen, and score 5 was given to an almost perfect nest, where > 90% of the nestlet was torn up into a crater where the walls were higher than the body height. Mean score ± SEM of each group was determined.

2.12.3. Marble burying testing

Aberrant marble burying behaviour is a sign of anxiety and repetitive behaviour in rodents (Deacon, 2012). Marble burying test was assessed in males at 19 weeks and in females at 18 weeks. Twelve glass marbles (1.5 cm in diameter) were placed, evenly spaced (3 × 4 rows), on a flat layer of 3 cm corn cob in the home cage (37.3 × 23.4 × 14.0 cm). A mouse was placed single caged and left for 30 min after which the number of marbles buried 2/3 were counted. Mean number of marbles buried ± SEM of each group were determined.

2.13. Statistical analyses

GraphPad Prism 7.05 was used to analyse all data (GraphPad Software Inc., San Diego, CA, USA). Shapiro-Wilk normality test was used to determine a Gaussian distribution. One-way or two-way factor analysis of variance (ANOVA) with Holm- Sidak post-hoc test, or Kruskal-Wallis with Dunn's post-hoc test was used for multiple comparisons. Student's unpaired *t*-test with Welch's correction was used analyzing number and size of inclusions in striatum and cortex. Results are presented as means ± SEM. *P*-values, F-values and degrees of freedom are presented for one- way and two-way ANOVA, and Student's unpaired t-test (Supplementary statistical results), giving the equality of means from each group. Differences with a $p < .05$ were considered statistically significant.

3. Results

3.1. Increased body weight and altered body composition in leptin-deficient R6/2 mice

To investigate whether it is possible to reverse the high metabolic state and body weight loss in HD, we utilized the well-characterized R6/2 mouse model. We used transgenic R6/2 mice with two different CAG repeat lengths (CAG $^{345–352}$ and CAG $^{242-257}$). The CAG repeat length corresponds to disease progression and results in a slower disease progression compared with R6/2 mice with 150 CAGs (Morton et al., 2009). We recently showed that R6/2 mice with 273–285 CAGs exhibit neuropathological changes, such as increased levels of CSF NfL and reduced striatal volume (Soylu-Kucharz et al., 2017) at 18 weeks of age.

R6/2 mice were placed on a leptin-deficient genetic background using a two-step breeding strategy (Supplementary Fig. 1). To investigate the effects of leptin-deficiency on body weight we assessed body weight twice weekly in male and female mice in two cohorts of leptin-deficient R6/2 mice (R6/2$^{(CAG\ 345–352)}$;Ob/Ob and R6/2$^{(CAG\ 242–257)}$;Ob/Ob). Supportive of previous studies, significantly lower body weight was seen in male R6/2$^{(CAG\ 345–352)}$ mice at 14.5 weeks of age ($p = .0473$) (Fig. 1A), and in female R6/2$^{(CAG\ 345–352)}$ mice at 14 weeks of age ($p = .02$) (Fig. 1B) compared to WT littermates. Similarly, significantly lower body weight was seen in male R6/2$^{(Cag\ 242–257)}$ mice at 9.5 weeks ($p = .0464$) (Fig. 1C) compared to WT mice and at 12 weeks in female R6/2$^{(Cag\ 242–257)}$ mice ($p = .0412$) (Fig. 1D).

Male and female R6/2 mice with a leptin-deficient genetic background (R6/2$^{(CAG\ 345-352)}$;Ob/Ob and R6/2$^{CAG\ 242–257}$;Ob/Ob) had a significantly higher body weight compared to R6/2 littermates throughout the study ($p > .0001$) (Fig. 1). Although body weight was significantly increased in both R6/2 strains on leptin-deficient genetic background, their body weight was starting to decline for both R6/2$^{(CAG\ 345–352)}$;Ob/Ob and R6/2$^{(CAG\ 242–257)}$;Ob/Ob (although still significantly higher than R6/2 mice and wild-type littermates) around the same time as R6/2 mice were exhibiting a significantly reduced body weight compared with wild-type littermates. Heterozygote leptin-deficiency (R6/2$^{(CAG\ 345–352)}$;Ob−/+ and R6/2$^{(CAG\ 242–257)}$;Ob−/+) was not sufficient to result in increased body weight (Supplementary Fig. 2A, 2B and 2C).

In R6/2 mice altered body composition has been described (She et al., 2011). We therefore assessed body composition using DEXA scan. Ob/Ob mice ($p > .0001$), as well as R6/2$^{(CAG\ 345–352)}$;Ob/Ob mice ($p > .0001$), exhibited dramatically increased fat mass compared to both wild-type mice and R6/2 mice (Fig. 2A and B). No effect on body composition was seen in R6/2$^{(CAG\ 345–352)}$;Ob−/+ male or female mice (Supplementary Fig. 3A and 3B).

Although fat mass was increased at both time points comparing leptin-deficient R6/2 mice to R6/2 mice and WT mice, male leptin-

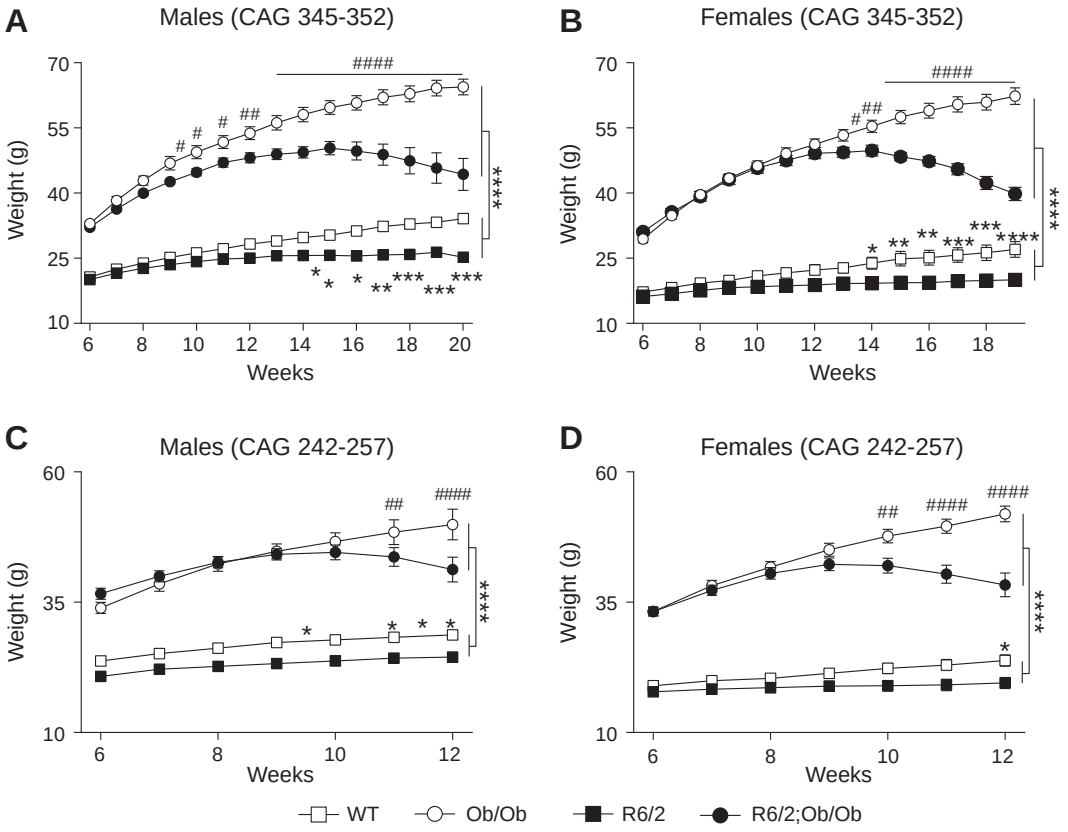

Fig. 1. Increased body weight in leptin-deficient R6/2 mice. Body weight was monitored up to 20 weeks in R6/2$^{(CAG\ 345–352)}$ cohort in males (A) and up to 19 weeks in females (B) (n = 7–9/genotype/gender). The changes in body weight of R6/2$^{(CAG\ 242–257)}$ cohort were followed up to 12 weeks in both males (C) and females (D) (n = 6–9/genotype/gender). Significantly lower body weight was seen in male R6/2$^{(CAG\ 345–352)}$ mice at 14.5 weeks of age (A), and in female R6/2$^{(CAG\ 345–352)}$ mice at 14 weeks of age (B) compared to WT littermates. Male and female R6/2 mice on a leptin- deficient genetic background (R6/2$^{(CAG\ 345–352)}$;Ob/Ob) (n = 7–9) have a significantly higher body weight compared with R6/2 littermates (A, B). Significantly lower body weight was seen in male R6/2$^{(CAG\ 242–257)}$ mice at 9.5 weeks of age (C), and in female R6/2$^{(CAG\ 345–352)}$ mice at 12 weeks of age (D) compared to WT littermates. R6/2$^{(CAG\ 242–257)}$ (male and female) mice on leptin- deficient genetic background also have a significantly higher weight compared to both wild type and R6/2$^{(CAG\ 242–257)}$ littermates (n = 6–9) (C, D). Data represent mean ± SEM. Statistical significance was determined by repeated measures of 2-way ANOVA with Holm-Sidak post hoc test for multiple comparisons. *p < .05, **p < .01, ****p < .0001.

deficient R6/2 mice demonstrated significantly lower fat mass compared with Ob/Ob mice at 16 (p = .0006) and 19 weeks (p > .0001) (Fig. 2A).

In contrast to the dramatic effect on fat mass, there was only a limited change in lean mass. A small but significant decrease in lean mass was seen in male R6/2$^{(CAG\ 345-352)}$;Ob/Ob mice compared to Ob/Ob littermates at 19 weeks (p = .0275) (Fig. 2C), however lean mass was not different comparing male R6/2$^{(CAG\ 345–352)}$ to R6/2$^{(CAG\ 345-352)}$;Ob/Ob mice. Lean mass was significantly reduced in female R6/2$^{(CAG\ 345–352)}$ at 18 weeks (p = .0398) compared to WT littermates (Fig. 2D). A small, but significant increase in lean mass was seen in female R6/2$^{(CAG\ 345–352)}$;Ob/Ob mice compared to R6/2$^{(CAG\ 345–352)}$ littermates at 15 weeks (p = .0308), however at 18 weeks there was no difference. Since skeletal muscle wasting is a known feature of HD and transcriptional changes in skeletal muscle have been demonstrated (Strand et al., 2005), we also assessed skeletal muscle gene expression. We did here not observe any significant change in mRNA levels of any of the genes evaluated (Supplementary Fig. 4).

In addition to the progressive weight loss seen in R6/2 mice, tissue weight has also been shown to be altered in R6/2 mice (Sathasivam et al., 1999). Tissue weight (brain, liver, kidneys) was here assessed in male leptin-deficient R6/2$^{(CAG\ 345–352)}$ mice and littermates at 20 weeks and in females at 19 weeks (Table 1). No change in tissue weight was seen in R6/2$^{(CAG\ 345–352)}$ compared to WT littermates. Leptin-deficiency resulted in higher liver and kidney weight, as well as longer body length, compared with WT and R6/2$^{(CAG\ 345–352)}$ littermates in both males and females (Table 1). Notably, brain weight was reduced in Ob/Ob females (p = .0116) and leptin- deficient R6/2$^{(CAG\ 345–352)}$ males (p = .0204) compared with their WT littermates (Table 1).

3.2. Decreased metabolic rate in leptin-deficient R6/2$^{(CAG\ 345–352)}$ mice

In R6/2 mice, body weight loss has been shown to be associated with high oxygen consumption (van der Burg et al., 2008). We therefore investigated whether leptin deficiency could restore the high energy expenditure state in R6/2 mice. We utilized the Pheno-master system in order to assess indirect gas calorimetry, food and water intake, as well as locomotor activity over 24 h in male mice at 15 weeks of age. Similar to previous studies (van der Burg et al., 2008), we found a tendency towards increased oxygen consumption, carbon oxide production, respiratory exchange rate and energy expenditure in R6/2$^{(CAG\ 345–352)}$ mice (Fig. 3A–D). In contrast, leptin-deficient R6/2 mice (R6/2$^{(CAG\ 345–352)}$;Ob/Ob males) exhibit a significant and profound reduction in respiratory exchange rate compared to R6/2$^{(CAG\ 345–352)}$ littermates (Fig. 3). The difference in respiratory exchange rate could not be explained by altered food or water consumption, as this was unaltered across the four groups assessed (Fig. 3E and F). Locomotor activity measurements were in line with previous findings (van der Burg et al., 2008) that no difference was seen in R6/2$^{(CAG\ 345–352)}$ mice compared to WT littermates. However, Ob/Ob and R6/2$^{(CAG\ 345-352)}$;Ob/Ob groups showed decreased activity compared to only WT littermates both during dark phase and 24 h (p < .0001) (Fig. 3G and H).

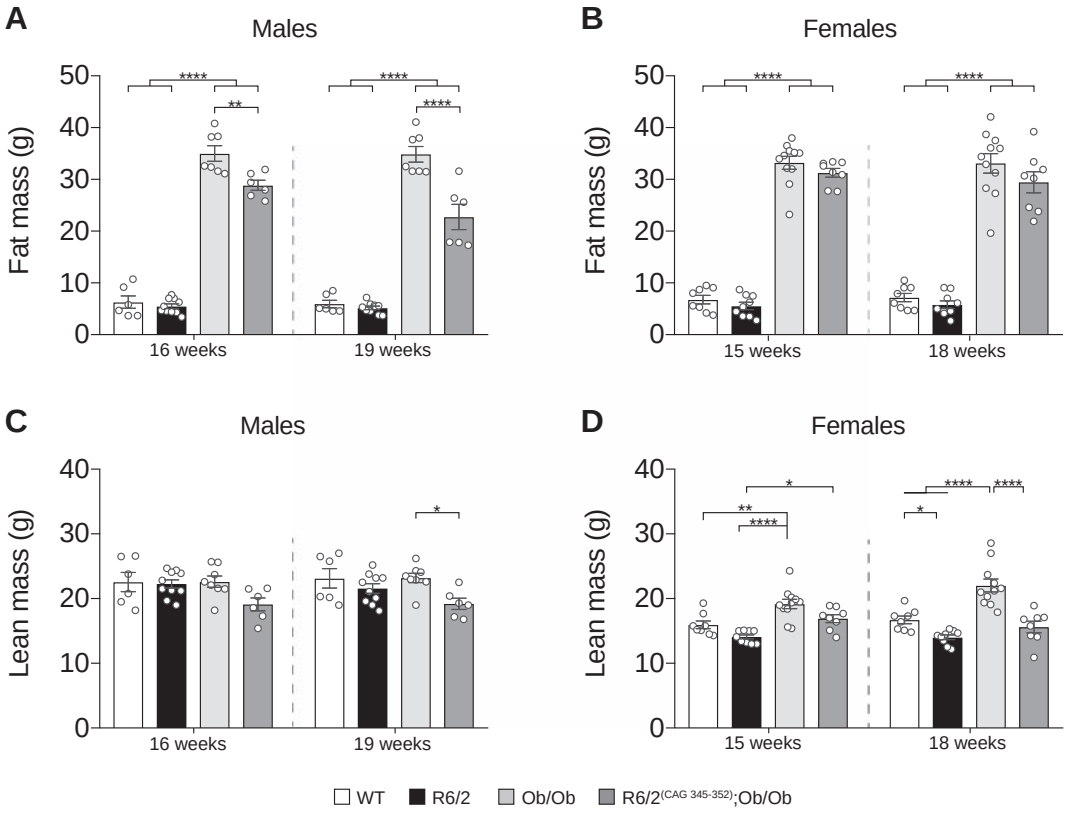

Fig. 2. Increased fat mass in leptin-deficient R6/2$^{(CAG\ 345–352)}$ mice. Assessment of body fat composition using DEXA scan in males (A) at 16 and 19 weeks (n = 6–10) and in females (B) (*n* = 8–11) at 15 and 18 weeks. There was a significant increase in fat mass in R6/2$^{(CAG\ 345–352)}$;Ob/Ob males (A) and females (B) compared to R6/2$^{(CAG\ 345–352)}$ littermates. A significant decrease in lean mass measurements was seen in R6/2$^{(CAG\ 345–352)}$;Ob/Ob male mice (C) at 19 weeks and the females mice (D) at 18 weeks compared to Ob/Ob littermates (C). Lean mass was not different in male R6/2$^{(CAG\ 345–352)}$ mice compared to R6/2$^{(CAG\ 345–352)}$;Ob/Ob mice (C). There was a significant reduction in lean mass in female R6/2$^{(CAG\ 345–352)}$ mice compared to WT littermates at 18 weeks of age (D). A significant increase in lean mass was seen in female R6/2$^{(CAG\ 345-\ 352)}$;Ob/Ob mice compared to R6/2$^{(CAG\ 345–352)}$ littermates at 15 weeks, however, at 18 weeks there was no difference (D). Data represent mean ± SEM. Statistical significance was determined by One-way ANOVA with Holm-Sidak post hoc test for multiple comparisons. A *p*-value below 0.05 was considered significant. *p < .05 and ****p < .0001.

3.3. White adipose tissue characteristics could contribute to the decreased energy expenditure found in leptin-deficient R6/2$^{(CAG\ 345–352)}$ mouse

Browning of WAT accompanied by an increase in adipocyte oxygen consumption, increased *Ucp1* (*uncoupling protein 1*) expression and adipocyte size changes, have been demonstrated in R6/2 mice (McCourt et al., 2016). We could here replicate these findings in R6/2$^{(CAG\ 345–352)}$ mice and show that WAT adipocytes were smaller compared to WT adipocytes (p < .0001) (Fig. 4C), with gene expression supporting browning (increased in *Ucp1* expression; *p* = .002) (Fig. 4D).

In contrast, the increased fat mass found in R6/2$^{(CAG\ 345–352)}$;Ob/Ob

Table 1
Effects on body and tissue weight in leptin-deficient R6/2$^{(CAG\ 345–352)}$ mice. Tissue and body weight, and body length in males at 20 weeks and in females at 19 weeks. Data are expressed as mean ± SEM. One-way ANOVA with Holm-Sidak post hoc test for multiple comparisons or Kruskal-Wallis with Dunn's post hoc test for multiple comparisons was used to analyse data. *Represents the p-value between WT and R6/2$^{(CAG\ 345–352)}$ mice, and #represents the p-value between R6/2$^{(CAG\ 345–352)}$;Ob/Ob and R6/2$^{(CAG\ 345–352)}$ mice, (n = 6–9). A p-value below 0.05 was considered significant.

Males - 20 weeks	WT	R6/2	Ob/Ob	R6/2;Ob/Ob	*p-value	#p-value
Body weight (g)	34.10 ± 1,08	25.23 ± 0.40	64.42 ± 1.81	44.31 ± 3.67	0.0063	< 0.0001
Length (cm)	9.09 ± 0.07	8.89 ± 0.07	9.79 ± 0.08	9.05 ± 0.12	> 0.9999	> 0.9999
Tissue weight (g)						
Brain	0.42 ± 0.007	0.41 ± 0.012	0.40 ± 0.005	0.38 ± 0.009	> 0.9999	0.323
Liver	1.12 ± 0.08	1.15 ± 0.05	4.24 ± 0.47	2.19 ± 0.20	> 0.999	0.091
Kidneys	0.35 ± 0.02	0.30 ± 0.01	0.45 ± 0.02	0.36 ± 0.02	0.136	0.095

Females - 19 weeks	WT	R6/2	Ob/Ob	R6/2;Ob/Ob	*p-value	#p-value
Body weight (g)	27.03 ± 1.80	20.04 ± 1.01	62.32 ± 1.90	39.80 ± 1.64	0.012	< 0.0001
Length (cm)	8.82 ± 0.10	8.44 ± 0.09	9.53 ± 0.07	9.04 ± 0.12	0.412	0.028
Tissue weight (g)						
Brain	0.43 ± 0.007	0.43 ± 0.011	0.39 ± 0.005	0.39 ± 0.011	> 0.999	0.211
Liver	0.76 ± 0.04	1.01 ± 0.08	3.83 ± 0.24	2.53 ± 0.18	> 0.999	0.843
Kidneys	0.25 ± 0.01	0.25 ± 0.01	0.37 ± 0.02	0.33 ± 0.01	> 0.999	0.060

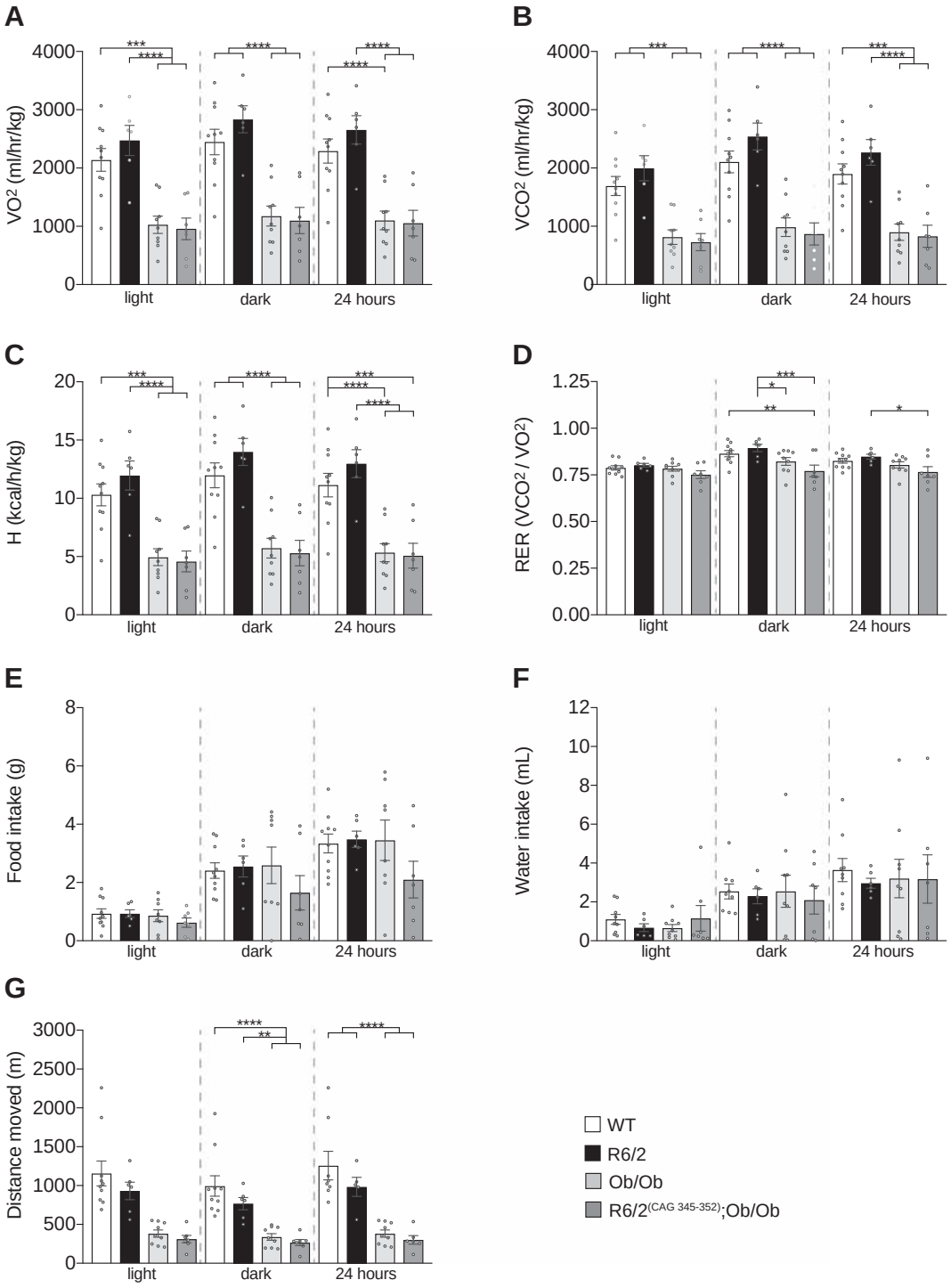

Fig. 3. Decreased metabolic rate in leptin-deficient R6/2$^{(CAG\ 345–352)}$ mice. Indirect Gas Calorimetry, as well as food and water intake, was measured over 24 h using the PhenoMaster/LabMaster Home cage System in males group at 15 weeks of age (n = 6–10/genotype). Oxygen consumption (A), carbon dioxide production (B), energy expenditure (C), respiratory rate (D), food and water intake, cumulative over 12 h light or dark phase or over 24 h (E, F), and locomotor activity (G) was assessed during light and dark phase, as well as expressed as over 24 h. R6/2$^{(CAG\ 345–352)}$;Ob/Ob males exhibit reduced metabolic rate compared to R6/2$^{(CAG\ 345–352)}$ littermates (A, B, C and D). The decrease in energy expenditure was not accompanied with change in food (E) and water intake (F). Ob/Ob and R6/2$^{(CAG\ 345–352)}$;Ob/Ob males exhibit decreased locomotor activity compared to WT and R6/2$^{(CAG\ 345–352)}$ littermates during dark phase and over 24 h (G). n = 6–10/group. Data represent mean ± SEM. One-way ANOVA with Holm-Sidak post hoc test for multiple comparisons. *$p < .05$, ****$p < .000$.

mice (Fig. 2A and B) was accompanied by increased size of adipocytes ($p < .0001$), as well as white adipocyte gene expression characteristics (increased in Hp expression; $p = .0147$) compared with R6/2(CAG 345–352) mice (Fig. 4C and D). WAT gene expression in leptin-deficient R6/2 mice displayed similar characteristics as those of Ob/Ob mice WAT, while WAT adipocytes were smaller compared to Ob/Ob littermates ($p = .0012$) (Fig. 4C and D).

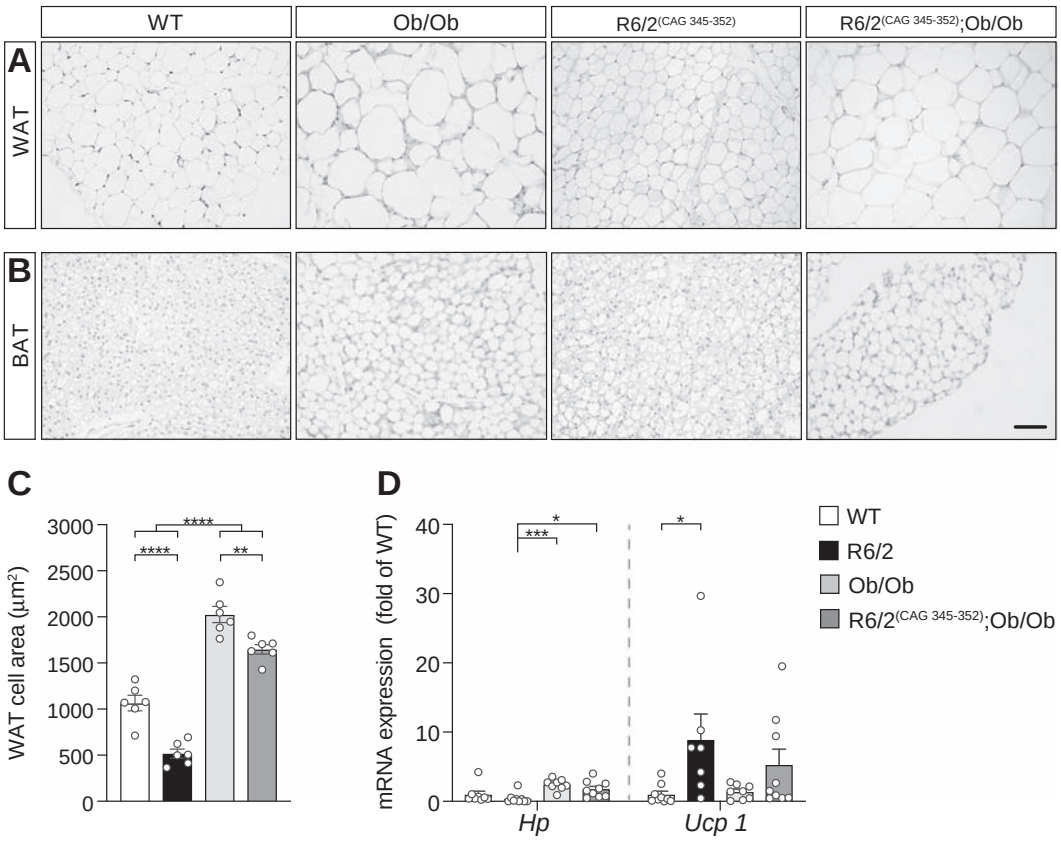

Fig. 4. White adipose tissue characteristics could contribute to the decreased energy expenditure found in leptin-deficient R6/2$^{(CAG\ 345–352)}$ mouse. Representative images of Hematoxylin-Eosin staining, showing the inguinal white adipose tissue (WAT) (A) and interscapular brown adipose tissue (BAT) (B) in males at 20 weeks. Stereological analysis of adipocyte cell area in male mice at 20 weeks (n = 6/genotype) by using cellSens Dimensions 1.11 software. Increased fat mass is present in R6/2$^{(CAG\ 345–352)}$;Ob/Ob mice (illustrated in Fig. 2). R6/2$^{(CAG\ 345–352)}$ mice white adipose tissue exhibit brown adipose tissue characteristics, with smaller WAT adipocytes (C). Assessments of *Hp* and *Ucp 1* mRNA changes in WAT of male mice at 20 weeks (n = 8–10/genotype), show an increased WAT expression of *Ucp1* in R6/2$^{(CAG\ 345–352)}$ mice compared to WT littermates (D). Importantly, leptin-deficient R6/2$^{(CAG\ 345–352)}$ mice exhibit white WAT characteristics, i.e. larger adipocytes (C), increased *Hp* expression and less *Ucp1* expression (D). Pro-white and pro-brown gene expression changes in WAT (n = 8–10) (D). ΔΔCt method was used to analyse gene expression and normalized to *TBP* and *Ppia*, and the data represented as mean ± SEM. One-way ANOVA with Holm-Sidak post hoc test for multiple comparisons. *p < .05, ***p < .001, ****p < .0001. (For interpretation of the references to colour in this figure legend, the reader is referred to the web version of this article.)

Table 2
Metabolic serum parameters in leptin-deficient R6/2$^{(CAG\ 345–352)}$ mice. Glucose and insulin levels were measured in males at 20 weeks, and pancreatic β- cell function and insulin resistance were calculated (n = 7–9/group). HDL and LDL/VLDL cholesterol levels were measured, and the (LDL/VLDL)/HDL ratio was calculated (n = 6/group). *Represents the p-value between WT and R6/2$^{(CAG\ 345–352)}$ mice, and #represents the p-value between R6/2$^{(CAG\ 345–352)}$;Ob/Ob and R6/2$^{(CAG\ 345–352)}$ mice. Data represent mean ± SEM. Statistical significance was determined by One-way ANOVA with Holm-Sidak post hoc test or Kruskal Wallis with Dunn's post hoc test for multiple comparisons. A p-value below 0.05 was considered significant.

Males - 20 weeks	WT	R6/2	Ob/Ob	R6/2;Ob/Ob	*p-Value	#p-Value
Glucose homeostasis						
Basal glucose (mmol/L)	2.13 ± 0.80	9.98 ± 1.77	6.67 ± 0.87	13.51 ± 1.09	0.002	0.095
Basal insulin (µg/L)	8.93 ± 1.57	2.94 ± 0.77	445.4 ± 73.31	49.61 ± 6.58	> 0.9999	0.006
HOMA-β	5958 ± 2543	209.3 ± 67.47	41,922 ± 12,955	2621 ± 647.0	0.085	0.045
HOMA-IR	20.13 ± 9.23	48.55 ± 17.78	3332 ± 814.2	791.2 ± 121.8	> 0.9999	0.051
Lipid homeostasis						
Total cholesterol (µg/µL)	0.65 ± 0.05	0.85 ± 0.06	0.94 ± 0.10	0.84 ± 0.12	0.451	0.947
HDL (µg/µL)	0.54 ± 0.04	0.60 ± 0.04	0.81 ± 0.09	0.67 ± 0.09	0.731	0.731
LDL/VLDL (µg/µL)	0.11 ± 0.01	0.25 ± 0.02	0.13 ± 0.02	0.17 ± 0.03	0.003	0.113
(LDL/VLDL): HDL ratio	0.21 ± 0.02	0.41 ± 0.02	0.17 ± 0.03	0.25 ± 0.02	< 0.0001	0.0003

3.4. Metabolic parameters in leptin-deficient R6/2$^{(CAG\ 345–352)}$ mice

We measured serum leptin levels in males at 20 weeks. As expected, leptin levels were below detection limit in serum from leptin-deficient Ob/Ob mice, as well as in serum from R6/2$^{(CAG\ 345–352)}$;Ob/Ob mice. Serum leptin levels were similar in R6/2$^{(CAG\ 345–352)}$ and WT mice (R6/2: 3.80 ± 0.93 ng/ml; $n = 8$ and WT: 4.97 ± 0.86 ng/ml; n = 8). Heterozygote leptin-deficiency (R6/2$^{(CAG\ 345–352)}$;Ob−/+ and Ob−/+) resulted in reduced, although not significant, leptin levels (R6/2$^{(CAG\ 345–352)}$;Ob−/+: 1142 ± 0,3805 ng/ml; $n = 6$ and Ob−/+: 2.604 ± 0.8415 ng/ml; n = 6). Similarly, central levels of leptin were below detection limit in Ob/Ob ($n = 3$), or close to detection limit in

R6/2$^{(CAG\ 345–352)}$;Ob/Ob 2.83 ± 2.83 pg/mg protein (n = 3). Central leptin levels were lower in R6/2 mice compared to WT mice (13.21 ± 6.54 pg/mg protein; $n = 5$ and 37.56 ± 10.07 pg/mg protein; $n = 4$ respectively).

Reduced plasma levels of insulin and accompanying hyperglycaemia have previously been demonstrated in R6/2 mice (Bjorkqvist et al., 2005). Therefore, serum glucose and insulin levels were measured in males at 20 weeks, and pancreatic β-cell function and insulin resistance were calculated to evaluate the effect of leptin- deficiency on glucose homeostasis in R6/2$^{(CAG\ 345–352)}$ mice. As previously shown (She et al., 2011), basal glucose levels were 4.7-fold higher ($p = .0016$) in R6/2$^{(CAG\ 345–352)}$ mice compared with WT littermates and similar in R6/2$^{(CAG\ 345–352)}$;Ob/Ob mice (Table 2). As expected, Ob/Ob mice, known to exhibit high insulin levels (Garris and Garris, 2004), had a 49.9-fold ($p = .0025$) higher basal insulin levels compared to WT littermates and 16.9-fold ($p = .006$) higher basal insulin level was seen in R6/2$^{(CAG\ 345–352)}$;Ob/Ob mice compared to R6/2$^{(CAG\ 345–352)}$ mice (Table 2).

β-cell function, presented as HOMA-β, was improved in R6/2$^{(CAG\ 345–352)}$;Ob/Ob (2621 ± 647; $n = 9$) mice compared with R6/2$^{(CAG\ 345–352)}$ littermates (209.3 ± 67.47; n = 9) ($p = .0449$). Increased insulin resistance, presented as HOMA-IR, was only seen in Ob/Ob (3332 ± 814.2; n = 9) mice compared to WT (20.13 ± 9.23; $n = 7$) ($p = .0001$) and R6/2$^{(CAG\ 345–352)}$ (48.55 ± 17.78; n = 9)($p = .0002$) mice (Table 2).

Fatty acid metabolites have previously been shown to be altered in HD (Leoni et al., 2011; Valenza et al., 2007). Therefore, we evaluated circulating levels of total cholesterol levels, HDL and LDL/VLDL cholesterol levels, and the ratio of LDL/VLDL and HDL was calculated (Table 2). Serum levels of total cholesterol and HDL were similar across all groups (Table 2). LDL/VLDL levels in R6/2$^{(CAG\ 345–352)}$ mice were 2.2-fold higher compared with WT littermates ($p = .0034$). The ratio between LDL/VLDL and HDL was higher in R6/2$^{(CAG\ 345–352)}$ mice compared to both wildtype mice ($p < .0001$) and R6/2$^{(CAG\ 345–352)}$;Ob/Ob mice ($p = .0003$).

3.5. Leptin-deficiency and increased body fat have no effect on R6/2 mouse neuropathology

NfL has been shown to be an axonal damage and cell death marker in neurodegenerative disease including HD (Byrne et al., 2017; Norgren et al., 2003). Recently, we have shown that both CSF and serum levels of NfL correlates with reduced striatal volume and body weight in R6/2 $^{(CAG\ 242–257)}$ mice (Soylu-Kucharz et al., 2017). To further investigate the influence of the increased body weight on R6/2 neuropathology, we quantified the CSF concentrations of NfL using an ultra-sensitive immunoassay (Rohrer et al., 2016; Soylu-Kucharz et al., 2017). We found increased levels of NfL in R6/2 (p = .0002) and R6/2$^{(CAG\ 345–352)}$; Ob/Ob (p = .0002) mice compared to Ob/Ob mice, whereas there was no significant change between WT compared to R6/2, Ob/Ob and R6/2$^{(CAG\ 345–352)}$;Ob/Ob genotypes (Fig. 5A).

Striatum, cortex and corpus callosum are affected in clinical and animal models of HD, and this loss of volume occurs as a result of progressive cellular dysfunction and, eventually, cell death (Rosas et al., 2010; Vonsattel, 2008). Here, we sought to investigate whether slowing down the metabolism, by crossing R6/2 mice with leptin- deficient mice, would prohibit the progressive neurodegeneration in R6/2 mice. First, we assessed gross neuropathological changes in all four genotypes WT, R6/2, Ob/Ob and R6/2$^{(CAG\ 345–352)}$;Ob/Ob mice. There was no significant change in striatal volume and cortex thickness among the four groups (Fig. 5B and C). The assessment of corpus callosum thickness showed a significant reduction in Ob/Ob mice compared with the WT group ($p = .0245$) (Fig. 5D). One of the hallmarks of the HD is inclusion formation and it is primarily associated with cell death (Davies et al., 1997; DiFiglia et al., 1997). The R6/2 mouse model featured these HD intranuclear and neuropil inclusions appearing earliest in the cortex and striatum (Meade et al., 2002). Therefore, we here quantified the number and size of inclusions in R6/2 and R6/2$^{(CAG\ 345–352)}$;Ob/Ob mice in both brain areas. There was no effect of increased BMI on the cortical and striatal inclusion formation (Fig. 5E–H). To further determine the neuropathological changes in this cross-breeding, we assessed mRNA levels of well-characterized transcriptionally dysregulated genes in the HD striata (Menalled et al., 2014). The gene expression assessments of *Darpp-32, Drd1a, Drd2,* and *Pda10a* showed no amelioration in the striatum of R6/2$^{(CAG\ 345–352)}$;Ob/Ob mice (Fig. 5K).

3.6. Limited effect on behaviour in leptin-deficient R6/2$^{(CAG\ 345–352)}$ mice

A battery of behavioural tests was employed to assess behaviour in males at 19 weeks and females at 18 weeks. At this age, there was no significant difference in distance travelled (open field) in between groups in either male (Fig. 6A) or female (Fig. 6B) mice. Nest building is a spontaneous and complex behaviour of mice, requiring fine motoric skills, as well as cognitive function (Deacon, 2012). Reduced nesting behaviour was seen in R6/2$^{(CAG\ 345–352)}$ males at 19 weeks ($p = .0074$) (Fig. 6C), and in R6/2$^{(CAG\ 345–352)}$ females at 18 weeks ($p < .0001$) (Fig. 6D) compared to WT littermates. No normalization was seen in leptin-deficient R6/2$^{(CAG\ 345–352)}$ males or females (Fig. 6C and D). Increased marble burying behaviour is a sign of anxiety and repetitive behaviour in rodents (Deacon, 2006a). Marble burying test was performed in males at 19 weeks and in females at 18 weeks. R6/2$^{(CAG\ 345–352)}$ male mice at 19 weeks (Fig. 6E) demonstrated significant ($p = .0169$) increase in marbles buried compared to wild- type littermates, this behavioural change was normalized in R6/2$^{(CAG\ 345–352)}$ mice on a leptin-deficient genetic background (p < .0001) (Fig. 6E).

4. Discussion

Accumulating evidence emphasize systemic metabolism alterations as key feature of HD pathology (Aziz et al., 2010; Carroll et al., 2015; van der Burg et al., 2009, 2011). Recently, a large observational study presented convincing evidence showing that a higher BMI is associated with a slower rate of disease progression in clinical HD, independent of CAG repeat length and disease stage (van der Burg et al., 2017). Energy homeostasis alterations seen in HD (Carroll et al., 2015; van der Burg et al., 2009, 2011), might be due to either central pathology, especially the hypothalamus (Petersen and Bjorkqvist, 2006; Petersen and Gabery, 2012) or peripheral tissue alterations (McCourt et al., 2016; Strand et al., 2005; van der Burg et al., 2009, 2011), or by a combination (Carroll et al., 2015).

Here we demonstrate that through a genetic approach it is possible to increase body weight and decrease whole-body energy metabolism in the transgenic R6/2 mouse model of HD. We placed R6/2 mice on a leptin-deficient (Ob/Ob) genetic background, thereby creating a mouse model exhibiting hypometabolism, with increased body weight and fat mass, as well as reduced oxygen consumption, CO_2 production, energy expenditure and respiratory exchange rate.

Similar to HD, ALS is associated with increased energy expenditure and weight loss as part of disease features (Lim et al., 2014; Vandoorne et al., 2018). Interestingly, similar to the strategy here chosen, Lim et al. could in 2014 show that placing the G93A mutant SOD1 mice, a well-established ALS mouse model, on a leptin-deficient genetic background reversed the catabolic state (Lim et al., 2014).

In addition to obesity, Ob/Ob mice are leptin-deficient and hypometabolic (Coleman, 1978; Garthwaite et al., 1980; Ingalls et al., 1996; Mayer et al., 1953). Here we can show that leptin-deficient R6/2 mice have reduced oxygen consumption, CO_2 production, energy expenditure and respiratory exchange rate during both the light and dark phase. As we also see dramatic alterations in white adipose tissue characteristics, a plausible explanation for the reduction in the expiratory exchange rate could lie within white adipose tissue.

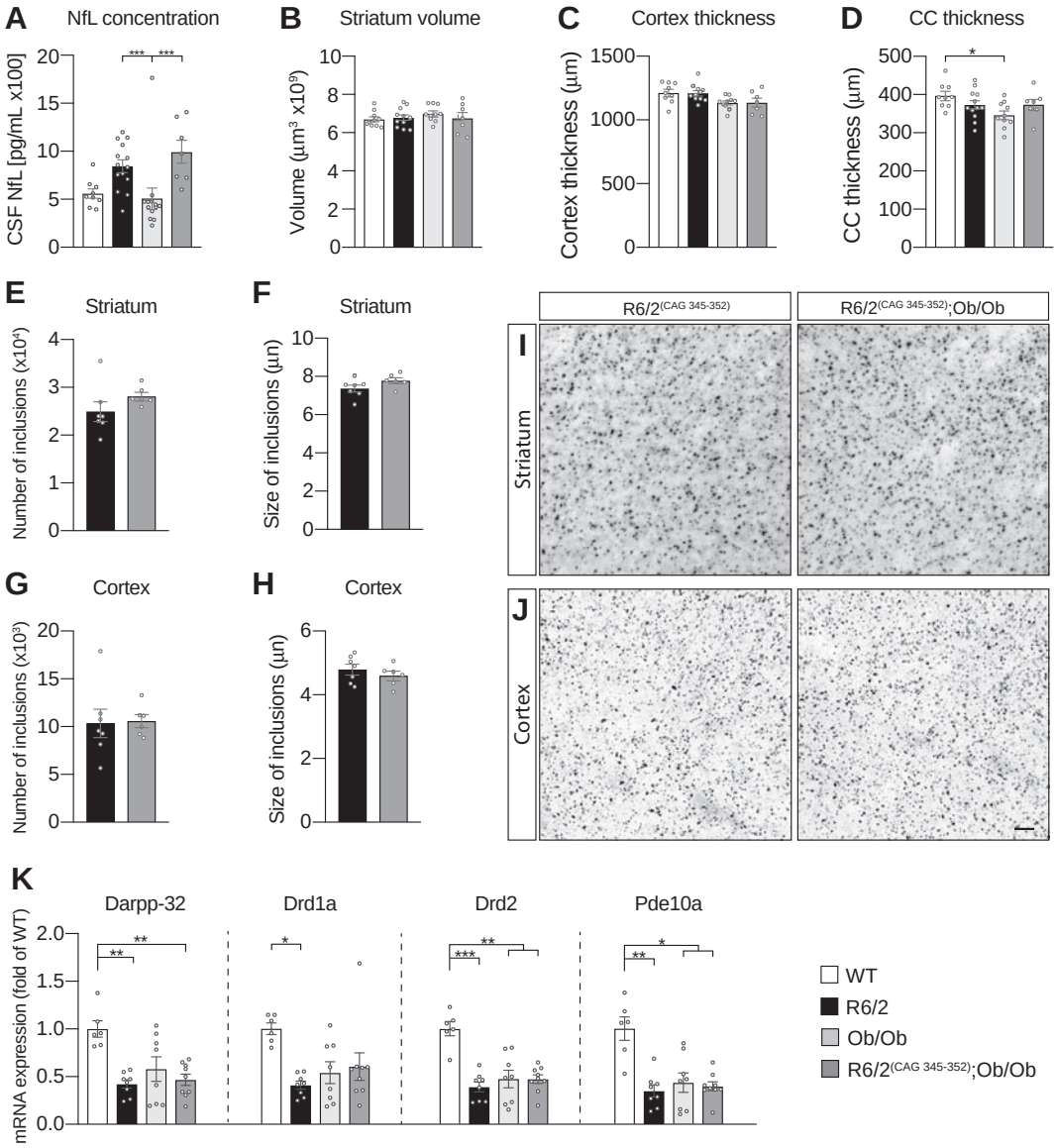

Fig. 5. Leptin-deficient R6/2 mice does not exhibit improved neuropathological measures. The CSF NfL concentrations were determined using a single molecule array (Simoa)-based immunoassay technology in male mice at 20 weeks (n = 8–14/group) (A). Measurement of striatum volume (B), cortical thickness (C) and corpus callosum thickness (D) in males at 20 weeks (n = 7–12/genotype). The size and number of inclusions assessed on R6/2 and the R6/2$^{(CAG\ 345–352)}$;Ob/Ob mice on EM48 (anti-HTT) strained brain sections. The number (E) and the size (F) of EM48 positive inclusions in the striatum (n = 6–7/genotype). Assessment of number (G) and size (H) of inclusions in the cortex (n = 6–7/genotype). Representative images are showing the HTT inclusions in the striatum (I) and cortex (J) of R6/2 and the R6/2$^{(CAG\ 345–352)}$;Ob/Ob mice. (K) Striatum mRNA levels of *Darpp- 32, Drd1a, Drd2, Pde10a* in 20 weeks old mice (n = 6–9/genotype). Data was normalized to mRNA of *actb* and *Atp5b* house-keeping gene and presented as a fold change in relation to wildtype mice. Scale bar represents 50 µm. Data represented as mean ± SEM. Statistical significance for stereological assessments and NfL levels were determined by One-way ANOVA with Holm-Sidak post hoc test for multiple comparisons, One-way ANOVA with Holm-Sidak post hoc test for multiple comparisons or Dunn's post hoc test was used analyzing striatal gene expression, and Student's unpaired *t*-test with Welch's correction was used analyzing number and size of inclusions in striatum and cortex.

Thermogenesis is an important physiological mechanism to produce heat and consume energy. In rodents, BAT is a major site of thermogenesis, where oxidation of fatty acids stimulates UCP1, a mitochondrial inner membrane protein that uncouples oxidative phosphorylation (Rousset et al., 2004). We have previously shown that R6/2 mouse white adipose tissue exhibit brown features, including *Ucp1* expression, and this is linked to an increase in adipocyte oxygen consumption (McCourt et al., 2016). The white adipose tissue of leptin-deficient R6/2 mice lacks signs of browning, likely contributing to decreased whole-body energy balance and the reduced RER.

The homozygote obese mutation, Ob/Ob, was first developed in an outbred mouse colony at the Jackson Laboratory, Bar Harbor, Maine in 1949 (Ingalls et al., 1996), and was backcrossed to the well-characterized C57BL mouse colony. Mice homozygous for the obese spontaneous mutation are first recognizable at four weeks of age, with increased food intake and rapid weight gain, which may reach four times the normal weight of wild-type controls (Ingalls et al., 1996; Szczypka et al., 2000).

Body weight in leptin-deficient R6/2 mice is dramatically increased compared to wildtype mice and R6/2 mice. Leptin-deficient R6/2 mice has a body weight gain curve comparable to that of leptin-deficient mice from 6 weeks to approximately 10 weeks of age. The increased body weight in Ob/Ob and R6/2 Ob/Ob mice, is likely also accompanied by increased food intake, as increased food intake has repeatedly been demonstrated in Ob/Ob mice (Szczypka et al., 2000). However, we did not in the cohort of mice used in this study detect a

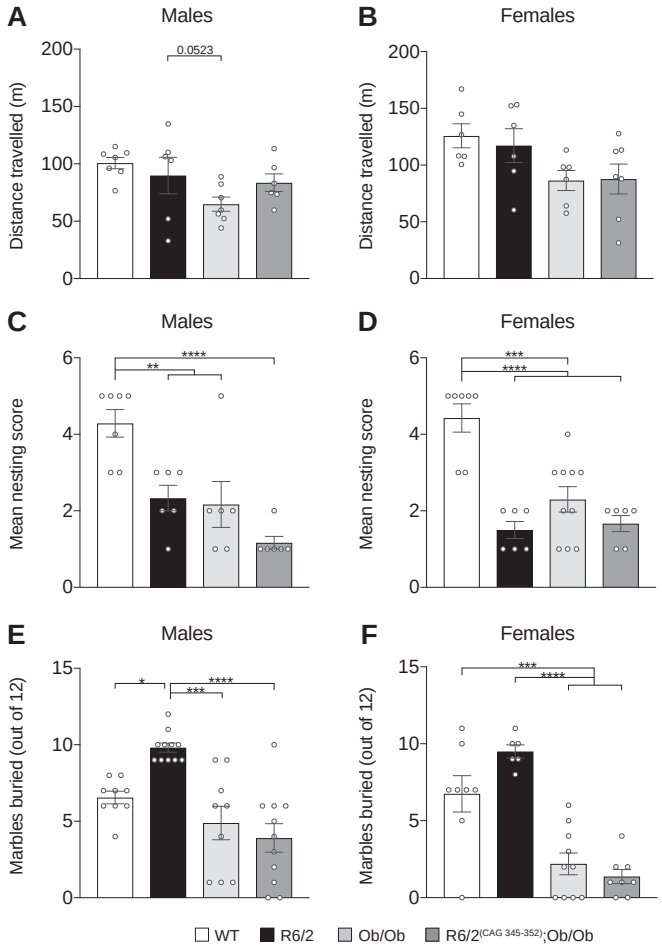

Fig. 6. Minor behavioural alterations in leptin-deficient R6/2$^{(CAG\ 345–352)}$ mice. Behaviour was assessed in males at 19 weeks and females at 18 weeks, prior to overt motoric changes, and at this age, there was no significant difference in distance travelled (open field) in between groups in either male (A) or female (B) mice (n = 6–7). A diminished nesting behaviour was seen in R6/2$^{(CAG\ 345–352)}$ males at 19 (n = 9–11) (C), and in R6/2$^{(CAG\ 345–352)}$ females at 18 (n = 6–10) (D) compared to WT littermates. No normalization was seen in R6/2$^{(CAG\ 345–352)}$ males or females on a leptin-deficient genetic background (R6/2$^{(CAG\ 345–352)}$;Ob/Ob) (C, D). Marble burying test was performed in males (n = 9–11) at 19 weeks (E) and in females (n = 6–10) at 18 weeks (F). R6/2$^{(CAG\ 345–352)}$ male mice at 19 weeks (E) demonstrated a significant increase in marbles buried compared on wild-type littermates, importantly, this behavioural change was normalized in R6/2$^{(CAG\ 345–352)}$ mice with a leptin-deficient genetic background (E). One-way ANOVA with Holm-Sidak post hoc test for multiple comparisons. *p < .05, **p < .001, ***p < .001, ****p < .0001.

change in food intake over 24 h when assessed using the PhenoMaster system. Likely, if we would have assessed food intake in home cage over a longer period, we would have seen a difference in food intake, as we see a dramatic increase in body weight.

Body weight gain seen in leptin-deficient mice and leptin-deficient R6/2 mice is likely due to increased fat mass as we see a dramatic increase in fat mas in leptin-deficient R6/2 mice. Lean mass was, with the here used genetic approach, only very marginally affected, illustrated also by no statistically significant change in skeletal muscle gene expression and the snout-to-anus length was comparable in all groups. In this study, two different R6/2 strains were used containing a CAG repeat between either 345–352 or 242–257. Both strains were crossed with leptin- deficient mice to generate leptin-deficient R6/2 with respective CAG repeats. We found similar results in term of increased body weight in both colonies. Our study illustrated that body weight changes are similar in both models used, and likely our results could be replicated in R6/2 models regardless of CAG repeat number.

HD is associated with progressive motoric and behavioural changes, with reduced ability to perform everyday tasks (Eddy and Rickards, 2013). Notably, van der Burg and colleagues showed in 2017 (van der Burg et al., 2017) that patients with a higher BMI at baseline exhibited a slower rate of progression assessed as functional capacity, motor function, and cognitive performance.

In our study, we have assessed activity and behaviour in mice prior to end stage disease, at a stage where striatal gene expression alterations are present, however not yet gross neuropathological alterations. As both leptin-deficient Ob/Ob and leptin-deficient R6/2 mice have a massive increase in body weight and the increased body weight is a confounding factor for testing of motor function, rotarod that is usually used to assessed motor function could not be used. Therefore, locomotor activity was assessed using two different approaches. In the first approach, the activity was analysed for 24 h along with indirect gas calorimetry measurements using the TSE phenomaster system, resulting in decreased activity in leptin-deficient Ob/Ob and leptin-deficient R6/2 mice. The decreased activity is probably due to obesity as it has been shown by others previously (Ahima et al., 1999; Joosten and van der Kroon, 1974). In the second approach, another cohort of mice was assessed using the open field arena, where only a trend of decreased activity was seen in Ob/Ob mice compared with WT mice. In an open filed arena, it is possible for mice testing that stress or being in a novel environment for a short period of time can lead to high variability in results. On the other hand, the automated assessment of activity over light/dark cycles provides robust results that are free from experimenter bias.

We have also tested mice for nest-building and marble burying behaviour. Nest-building behaviour in mice requires organization of a complex set of behaviours, such as fine motoric skills, as well as cognitive function (Deacon, 2012), and the ability of nest-building has been shown to be affected in both Alzheimer (Deacon et al., 2008) and Parkinson mouse models (Paumier et al., 2013). In the present study, we replicate our previous results (Sjögren et al., 2017) that R6/2 mice display reduced nest-building behaviour compared to WT littermates. However, no improvement was seen in leptin-deficient R6/2 mice, indicating that increased body weight and fat mass is not enough to affect this behavioural aspect in the R6/2 mouse.

Psychiatric manifestations such as obsessive-compulsion behaviour (OCD) and anxiety-like behaviour have been previously shown in patients with HD, preceding motor dysfunctions (Epping et al., 2016; Paulsen et al., 2017). Aberrant marble burying behaviour is a sign of anxiety and repetitive behaviour in rodents (Deacon, 2012). Here, we observed an increase in marbles buried in R6/2 mice compared with wild-type littermates, suggesting repetitive and anxiety-like behaviour (Deacon, 2006b). In agreement with previous studies (Ahima et al., 1999; Joosten and van der Kroon, 1974), reduced activity was here seen in both leptin-deficient and leptin-deficient R6/2 mice using the automated home cage phenotyping system. As both Ob/Ob and leptin-deficient R6/2 mice have demonstrated reduced locomotor activity and leptin-deficient R6/2 mice had no ameliorations in CNS pathology, the decreased number of marbles buried could be the potential confounds of obesity rather than a normalization of the behavioural phenotype. Apart from leptin function on food intake regulation, leptin is also involved in both pre- and postnatal development of cortex, neurite outgrowth and genetic ablation of leptin results in cognitive impairment (Udagawa et al., 2007; Oldreive et al., 2008). Therefore, we can speculate that reduced ability to form a nest could be the result of cortical impairments due to lack of leptin in both Ob/Ob and R6/2$^{(CAG\ 345–352)}$;Ob/Ob mice.

BMI is a measure of body weight with respect to height and it does not distinguish between fat and lean mass. Given that increased BMI correlates with disease- slowing effects in clinical HD (van der Burg et al., 2017) and the increase in BMI could be due to an increase in fat mass, we aimed to understand whether increase in fat mass can play a

neuroprotective role in R6/2 mice. To assess the gross neuropathological changes, we have measured striatal volume, cortex and corpus callosum thickness at 20 weeks. The striatal volume and cortex thicknesses were similar in all animals. It should be noted, however, that volumetric measurements do not provide information about cellular pathology and their functions. Therefore, in order to better characterize the effect of R6/2 mice on leptin-deficient genetic background, additional stereological analysis on specific cell populations would need to be performed. Corpus callosum is one of the largest white matter structures in the brain and several imaging studies showed reduced white matter volume already in pre-manifest HD subjects (Poudel et al., 2015; Zhang et al., 2018). Complementarily, we have previously shown a significant reduction in corpus callosum thickness in 18 weeks old R6/2 mice containing CAG repeat between 242 and 257 (Soylu-Kucharz et al., 2017). Yet, in this study, the absence of corpus callosum neuropathology in 20 weeks old R6/2 mice might be due to the elongated CAG repeats (345–352 CAG), as increased CAG repeat length is correlated with delayed pathology in the R6/2 mouse model of HD (Morton et al., 2009). Knowing that robust white matter pathology is indicative of axonal degeneration in HD and CSF NfL concentrations are a reliable predictor of HD neuropathology in both R6/2 animal model and clinical HD, we assessed the NfL levels in the CSF. Similar to the histopathological results, there was no significant change in CSF NfL levels between WT and HD mice groups (R6/2 and R6/2 mice on leptin-deficient genetic background). However, when we use an unpaired *t*-test to compare only R6/2 and WT groups, we found a significant increase in R6/2 CSF NfL levels (WT: $n = 9$, mean = 561 ng/ml, SEM = 47.5 and R6/2: $n = 14$, mean = 846.5 ng/ml, SEM = 65.3, two-tailed, unpaired t-test, $p = .002$), which was in line with our previous results (Soylu-Kucharz et al., 2017). This suggests that 20 weeks might not be a long enough time to provide a full picture of the neuropathological effects, although striatal gene expression alterations are found. Following the gross pathological assessment experiments, we quantified number and size of the mutant HTT inclusions and there was no significant effect of genotype. However, we found a trend towards an increase in the number of inclusions in R6/2;Ob/Ob compared with R6/2 mice. Even though it is not fully known whether the HTT inclusions are protective or toxic, there is strong evidence for the inclusions causing transcriptional dysregulation and disruption of cellular trafficking (Li et al., 2001; Passani et al., 2000). Therefore, we can postulate that higher body fat content can interfere with inclusion clearance as the obese phenotype is also closely associated with increased ER stress, which hinders misfolded protein degradation (Pagliassotti et al., 2016).

Transcriptional dysregulation in striatal signature genes, such as *Darpp-32, Drd1a, Drd2* and *Pda10a*, have been repeatedly shown in clinical HD and animal models (Desplats et al., 2006; Menalled et al., 2014). Our gene expression data showing the downregulation of these genes further confirms that increasing body fat and lowering the metabolic rate in R6/2 mice do not have a neuroprotective role in the progression of HD. One of the reasons could be the already ongoing brain pathology in Ob/Ob genetic background (Bereiter and Jeanrenaud, 1979). The Ob/Ob mice have significantly decreased brain weight (~15% loss) and volume with myelination deficits (Bereiter and Jeanrenaud, 1979; Sena et al., 1985), which can exacerbate HD pathology and potentially mask the beneficiary effects of reduced metabolic rate and weight loss.

Notably, in contrast to our results, Lim et al. could show beneficial effects on motor neurons in addition to reversal of the catabolic state in leptin-deficient ALS mice (Lim et al., 2014). We could speculate that a longer assessment might reveal changes in the brain pathology in our model, however lack of effect on R6/2 striatal gene expression profile speaks against this.

Taken together, no improvement of neuropathology in leptin-deficient R6/2 mice suggest that the disease onset delaying effect, linked to increased BMI in clinical HD, could be due to beneficial effects of lean mass rather than fat mass.

Our study has certain limitations. First, although our findings demonstrate the possibility of shifting energy metabolism from high to low and to increase body weight as well as post-pone body weight loss in the R6/2 mouse model, our study is massively shifting body composition with increased fat mass as a result, with only minor effects on lean mass. The leptin-deficient Ob/Ob mouse displays progressive metabolic alterations (Garthwaite et al., 1980; Mayer et al., 1953; Panchal and Brown, 2011) alongside early body weight gain and increased white adipose tissue depots (Dubuc, 1976). In addition to obesity, Ob/Ob mice are hyperinsulinemic at 4 weeks of age, transient hyperglycaemic from 4 to 12 weeks (Coleman, 1978; Garthwaite et al., 1980; Genuth et al., 1971; Mayer et al., 1953). The body weight increase precedes altered carbohydrate metabolism alterations that become noticeable at 4 weeks (Dubuc, 1976). The R6/2 mice also display dysregulated glucose metabolism, with mid-disease insulin-resistance progressing towards insulin-dependent diabetes (Andreassen et al., 2002; Bjorkqvist et al., 2005, 2006). In the leptin-deficient R6/2 mouse that we here created, glucose metabolism alterations are complex and this could influence whole body metabolism as well as possibly influencing brain pathology. R6/2 mice have previously been shown to display insulin resistance (Bjorkqvist et al., 2006) and in leptin-deficient R6/2 mice the insulin resistance is dramatically increased. It can't be excluded that this could lead to additional pathology in leptin-deficient R6/2 mice, as insulin-resistance has repeatedly been shown to be connected to neurodegeneration (Verdile et al., 2015).

The R6/2 colonies used in this study, have long CAG repeats and as previously shown therefore a slower progressing phenotype (Morton et al., 2009). As we have ended the study at an early R6/2 disease stage (prior to gross central atrophy, severe motor dysfunction and dramatic weight loss), but at a time point where neuropathology is present (R6/2 striatal gene expression is altered) this should make it possible to draw conclusion about the impact of body weight gain, prior to severe glucose balance alterations.

It might have been more beneficial with a slow switch of energy metabolism and a switch towards more lean mass. Secondly, although our study investigates a genetic approach to intervening in the disease course, our study is observational and does not provide full mechanistic explanation for how energy metabolism is altered. That high BMI is associated with slower disease progression (van der Burg et al., 2017), emphasize the importance of nutritional status, energy homeostasis and body composition from a clinical perspective. With this scenario, our findings provide important knowledge to further understand how shifting energy balance will affect HD. Future strategies focusing on restoring lean mass could possibly provide better understanding on the relevance of body composition for disease progression.

5. Conclusion

In conclusion, increasing body weight, by increasing white adipose tissue mass and lowering respiratory exchange rate in the R6/2 mouse model is not sufficient to generate neuroprotection. Our results encourage future studies focusing on restoring energy metabolism in HD, with alternative approaches.

Funding

This study was supported by Swedish Research Council (#2017-01080), Olle Engkvist Foundation, Royal Physiographic Society, Kocks foundation and Påhlsson foundation; Rana Soylu-Kucharz was supported by Swedish Brain Foundation postdoctoral fellowship grant. HZ is a Wallenberg Academy Fellow supported by grants from the Swedish Research Council (#2018-02532), the European Research Council (#681712) and Swedish State Support for Clinical Research (#ALFGBG-720931) and the UK Dementia Research Institute at UCL.

Contribution statement

M.B., M.S. and R.S.K. conceived and designed the experiments. M.S., R.S.K., U.D., T.L.S., M.C, Å.S. and H.Z. performed the experiments and analysed the data. M.B.,

M.S. and R.S.K. wrote the first draft of the manuscript. All authors reviewed the manuscript and approved the final version.

Declaration of Competing Interest

The authors declare that there are no conflicts of interest.

Acknowledgements

We thank Alicja Flasch, Ann-Charlotte Selberg and Susanne Jonsson for valuable technical assistance.

Research data

All data generated or analysed during this study is included in this published article, and its supplementary dataset.

Appendix A. Supplementary data

Supplementary data to this article can be found online at https://doi.org/10.1016/j.nbd.2019.104560.

References

Ahima, R.S., Bjorbaek, C., Osei, S., Flier, J.S., 1999. Regulation of neuronal and glial proteins by leptin: implications for brain development. Endocrinology 140, 2755–2762. https://doi.org/10.1210/endo.140.6.6774.

Andreassen, O.A., Dedeoglu, A., Ferrante, R.J., Jenkins, B.G., Ferrante, K.L., Thomas, M., Friedlich, A., Browne, S.E., Schilling, G., Borchelt, D.R., Hersch, S.M., Ross, C.A., Beal, M.F., 2001. Creatine increase survival and delays motor symptoms in a transgenic animal model of Huntington's disease. Neurobiol. Dis. 8, 479–491. https://doi.org/10.1006/nbdi.2001.0406.

Andreassen, O.A., Dedeoglu, A., Stanojevic, V., Hughes, D.B., Browne, S.E., Leech, C.A., Ferrante, R.J., Habener, J.F., Beal, M.F., Thomas, M.K., 2002. Huntington's disease of the endocrine pancreas: insulin deficiency and diabetes mellitus due to impaired insulin gene expression. Neurobiol. Dis. 11, 410–424. https://doi.org/10.1006/nbdi.2002.0562.

Aziz, N.A., Pijl, H., Frolich, M., Snel, M., Streefland, T.C., Roelfsema, F., Roos, R.A., 2010. Systemic energy homeostasis in Huntington's disease patients. J. Neurol. Neurosurg. Psychiatry 81, 1233–1237. https://doi.org/10.1136/jnnp.2009.191833.

Bartelt, A., Heeren, J., 2014. Adipose tissue browning and metabolic health. Nat. Rev. Endocrinol. 10, 24–36. https://doi.org/10.1038/nrendo.2013.204.

Bates, G.P., Dorsey, R., Gusella, J.F., Hayden, M.R., Kay, C., Leavitt, B.R., Nance, M., Ross, C.A., Scahill, R.I., Wetzel, R., Wild, E.J., Tabrizi, S.J., 2015. Huntington disease. Nat. Rev. Dis. Prim. 1, 15005. https://doi.org/10.1038/nrdp.2015.5.

Bereiter, D.A., Jeanrenaud, B., 1979. Altered neuroanatomical organization in the central nervous system of the genetically obese (ob/ob) mouse. Brain Res. 165, 249–260. https://doi.org/10.1016/0006-8993(79)90557-2.

Bjorkqvist, M., Fex, M., Renstrom, E., Wierup, N., Petersen, A., Gil, J., Bacos, K., Popovic, N., Li, J.Y., Sundler, F., Brundin, P., Mulder, H., 2005. The R6/2 transgenic mouse model of Huntington's disease develops diabetes due to deficient beta-cell mass and exocytosis. Hum. Mol. Genet. 14, 565–574. https://doi.org/10.1093/hmg/ddi053.

Bjorkqvist, M., Petersen, A., Bacos, K., Isaacs, J., Norlen, P., Gil, J., Popovic, N., Sundler, F., Bates, G.P., Tabrizi, S.J., Brundin, P., Mulder, H., 2006. Progressive alterations in the hypothalamic-pituitary-adrenal axis in the R6/2 transgenic mouse model of Huntington's disease. Hum. Mol. Genet. 15, 1713–1721. https://doi.org/10.1093/hmg/ddl094.

van der Burg, J.M., Bacos, K., Wood, N.I., Lindqvist, A., Wierup, N., Woodman, B., Wamsteeker, J.I., Smith, R., Deierborg, T., Kuhar, M.J., Bates, G.P., Mulder, H., Erlanson-Albertsson, C., Morton, A.J., Brundin, P., Petersen, A., Bjorkqvist, M., 2008. Increased metabolism in the R6/2 mouse model of Huntington's disease. Neurobiol. Dis. 29, 41–51. https://doi.org/10.1016/j.nbd.2007.07.029.

van der Burg, J.M., Bjorkqvist, M., Brundin, P., 2009. Beyond the brain: widespread pathology in Huntington's disease. Lancet Neurol. 8, 765–774. https://doi.org/10.1016/S1474-4422(09)70178-4.

van der Burg, J.M., Winqvist, A., Aziz, N.A., Maat-Schieman, M.L., Roos, R.A., Bates, G.P., Brundin, P., Bjorkqvist, M., Wierup, N., 2011. Gastrointestinal dysfunction contributes to weight loss in Huntington's disease mice. Neurobiol. Dis. 44, 1–8. https://doi.org/10.1016/j.nbd.2011.05.006.

van der Burg, J.M.M., Gardiner, S.L., Ludolph, A.C., Landwehrmeyer, G.B., Roos, R.A.C., Aziz, N.A., 2017. Body weight is a robust predictor of clinical progression in Huntington disease. Ann. Neurol. 82, 479–483. https://doi.org/10.1002/ana.25007.

Byrne, L.M., Rodrigues, F.B., Blennow, K., Durr, A., Leavitt, B.R., Roos, R.A.C., Scahill, R.I., Tabrizi, S.J., Zetterberg, H., Langbehn, D., Wild, E.J., 2017. Neurofilament light protein in blood as a potential biomarker of neurodegeneration in Huntington's disease: a retrospective cohort analysis. Lancet Neurol. 16, 601–609. https://doi.org/10.1016/S1474-4422(17)30124-2.

Carroll, J.B., Bates, G.P., Steffan, J., Saft, C., Tabrizi, S.J., 2015. Treating the whole body in Huntington's disease. Lancet Neurol. 14, 1135–1142. https://doi.org/10.1016/S1474-4422(15)00177-5.

Coleman, D.L., 1978. Obese and diabetes: two mutant genes causing diabetes-obesity syndromes in mice. Diabetologia 14, 141–148.

Coughlan, K.S., Halang, L., Woods, I., Prehn, J.H., 2016. A high-fat jelly diet restores bioenergetic balance and extends lifespan in the presence of motor dysfunction and lumbar spinal cord motor neuron loss in TDP-43A315T mutant C57BL6/J mice. Dis. Model. Mech. 9, 1029–1037. https://doi.org/10.1242/dmm.024786.

Davies, S.W., Turmaine, M., Cozens, B.A., DiFiglia, M., Sharp, A.H., Ross, C.A., Scherzinger, E., Wanker, E.E., Mangiarini, L., Bates, G.P., 1997. Formation of neuronal intranuclear inclusions underlies the neurological dysfunction in mice transgenic for the HD mutation. Cell 90, 537–548. https://doi.org/10.1016/S0092-8674(00)80513-9.

Deacon, R.M., 2006a. Assessing nest building in mice. Nat. Protoc. 1, 1117–1119. https://doi.org/10.1038/nprot.2006.170.

Deacon, R.M., 2006b. Digging and marble burying in mice: simple methods for in vivo identification of biological impacts. Nat. Protoc. 1, 122–124. https://doi.org/10.1038/nprot.2006.20.

Deacon, R., 2012. Assessing burrowing, nest construction, and hoarding in mice. J. Vis. Exp. e2607. https://doi.org/10.3791/2607.

Deacon, R.M., Cholerton, L.L., Talbot, K., Nair-Roberts, R.G., Sanderson, D.J., Romberg, C., Koros, E., Bornemann, K.D., Rawlins, J.N., 2008. Age-dependent and -independent behavioral deficits in Tg2576 mice. Behav. Brain Res. 189, 126–138. https://doi.org/10.1016/j.bbr.2007.12.024.

Dedeoglu, A., Kubilus, J.K., Yang, L., Ferrante, K.L., Hersch, S.M., Beal, M.F., Ferrante, R.J., 2003. Creatine therapy provides neuroprotection after onset of clinical symptoms in Huntington's disease transgenic mice. J. Neurochem. 85, 1359–1367. https://doi.org/10.1046/j.1471- 4159.2003.01706.x.

Desplats, P.A., Kass, K.E., Gilmartin, T., Stanwood, G.D., Woodward, E.L., Head, S.R., Sutcliffe, J.G., et al., 2006. Selective deficits in the expression of striatal-enriched mRNAs in Huntington's disease. J. Neurochem. 96, 743–757. https://doi.org/10.1111/j.1471-4159.2005.03588.x.

DiFiglia, M., Sapp, E., Chase, K.O., Davies, S.W., Bates, G.P., Vonsattel, J.P., Aronin, N., 1997. Aggregation of huntingtin in neuronal intranuclear inclusions and dystrophic neurites in brain. Science 277, 1990–1993. https://doi.org/10.1126/science.277.5334.1990.

Dubuc, P.U., 1976. The development of obesity, hyperinsulinemia, and hyperglycemia in ob/ob mice. Metab. Clin. Exp. 25, 1567–1574. https://doi.org/10.1016/0026-0495(76)90109-8.

Dupuis, L., Pradat, P.F., Ludolph, A.C., Loeffler, J.P., 2011. Energy metabolism in amyotrophic lateral sclerosis. Lancet Neurol. 10, 75–82. https://doi.org/10.1016/S1474-4422(10)70224-6.

Eddy, C.M., Rickards, H.E., 2013. Impact of cognitive and behavioural changes on quality of life in Huntington's disease. Basal Ganglia 3, 123–126. https://doi.org/10.1016/j.baga.2013.01.085.

Epping, E.A., Kim, J.I., Craufurd, D., Brashers-Krug, T.M., Anderson, K.E., McCusker, E., Luther, J., Long, J.D., Paulsen, J.S., Investigators P-H, Coordinators of the Huntington Study G, 2016. Longitudinal psychiatric symptoms in prodromal Huntington's disease: a decade of data. Am. J. Psychiatry 173, 184–192. https://doi.org/10.1176/appi.ajp.2015.14121551.

Franklin, K.B.J., Paxinos, G., 2008. The Mouse Brain in Stereotaxic Coordinates. Acad. Press, Amsterdam.

Garris, D.R., Garris, B.L., 2004. Cytochemical analysis of pancreatic islet hypercytolipidemia following diabetes (db/db) and obese (ob/ob) mutation expression: influence of genomic background. Pathobiology 71, 231–240. https://doi.org/10.1159/000080056.

Garthwaite, T.L., Martinson, D.R., Tseng, L.F., Hagen, T.C., Menahan, L.A., 1980. A longitudinal hormonal profile of the genetically obese mouse. Endocrinology 107, 671–676. https://doi.org/10.1210/endo-107-3-671.

Genuth, S.M., Przybylski, R.J., Rosenberg, D.M., 1971. Insulin resistance in genetically obese, hyperglycemic mice. Endocrinology 88, 1230–1238. https://doi.org/10.1210/endo-88-5-1230.

Goodman, A.O., Murgatroyd, P.R., Medina-Gomez, G., Wood, N.I., Finer, N., Vidal-Puig, A.J., Morton, A.J., Barker, R.A., 2008. The metabolic profile of early Huntington's disease–a combined human and transgenic mouse study. Exp. Neurol. 210, 691–698. https://doi.org/10.1016/j.expneurol.2007.12.026.

Gould, T.D.D.D.T., Kovacsics, C.E., 2009. The Open Field Test. Springer Links. Humana Press, Totowa, NJ.

Group THsDCR, 1993. A novel gene containing a trinucleotide repeat that is expanded and unstable on Huntington's disease chromosomes. Cell 72, 971–983. https://doi.org/10.1016/0092-8674(93)90585-E.

Hickey, M.A., Gallant, K., Gross, G.G., Levine, M.S., Chesselet, M.F., 2005. Early behavioral deficits in R6/2 mice suitable for use in preclinical drug testing. Neurobiol. Dis. 20, 1–11. https://doi.org/10.1016/j.nbd.2005.01.024.

Ingalls, A.M., Dickie, M.M., Snell, G.D., 1996. Obese, a new mutation in the house mouse. Obes. Res. 4, 101. https://doi.org/10.1002/j.1550-8528.1996.tb00519.x.

Joosten, H.F., van der Kroon, P.H., 1974. Growth pattern and behavioral traits associated with the development of the obese-hyperglycemic syndrome in mice (ob-ob). Metab. Clin. Exp. 23, 1141–1147. https://doi.org/10.1016/0026-0495(74)90030-4.

Leoni, V., Mariotti, C., Nanetti, L., Salvatore, E., Squitieri, F., Bentivoglio, A.R., Bandettini

del Poggio, M., et al., 2011. Whole body cholesterol metabolism is impaired in Huntington's disease. Neurosci. Lett. 494, 245–249. https://doi.org/10.1016/j.neulet.2011.03.025.
Li, H., Li, S.H., Yu, Z.X., Shelbourne, P., Li, X.J., 2001. Huntingtin aggregate-associated axonal degeneration is an early pathological event in Huntington's disease mice. J. Neurosci. 21, 8473–8481. https://doi.org/10.1523/JNEUROSCI.21-21-08473.2001.
Li, J.Y., Popovic, N., Brundin, P., 2005. The use of the R6 transgenic mouse models of Huntington's disease in attempts to develop novel therapeutic strategies. NeuroRx 2, 447–464. https://doi.org/10.1602/neurorx.2.3.447.
Lim, M.A., Bence, K.K., Sandesara, I., Andreux, P., Auwerx, J., Ishibashi, J., Seale, P., Kalb, R.G., 2014. Genetically altering organismal metabolism by leptin-deficiency benefits a mouse model of amyotrophic lateral sclerosis. Hum. Mol. Genet. 23, 4995–5008. https://doi.org/10.1093/hmg/ddu214.
Maffei, M., Halaas, J., Ravussin, E., Pratley, R.E., Lee, G.H., Zhang, Y., Fei, H., et al., 1995. Leptin levels in human and rodent: measurement of plasma leptin and ob RNA in obese and weight- reduced subjects. Nat. Med. 11, 1155–1161.
Matthews, D.R., Hosker, J.P., Rudenski, A.S., Naylor, B.A., Treacher, D.F., Turner, R.C., 1985. Homeostasis model assessment: insulin resistance and beta-cell function from fasting plasma glucose and insulin concentrations in man. Diabetologia 28, 412–419.
Mayer, J., Russell, R.E., Bates, M.W., Dickie, M.M., 1953. Metabolic, nutritional and endocrine studies of the hereditary obesity-diabetes syndrome of mice and mechanism of its development. Metab. Clin. Exp. 2, 9–21.
McCourt, A.C., Jakobsson, L., Larsson, S., Holm, C., Piel, S., Elmer, E., Bjorkqvist, M., 2016. White adipose tissue browning in the R6/2 mouse model of Huntington's disease. PLoS One 11, e0159870. https://doi.org/10.1371/journal.pone.0159870.
Meade, C.A., Deng, Y.P., Fusco, F.R., Del Mar, N., Hersch, S., Goldowitz, D., Reiner, A., 2002. Cellular localization and development of neuronal intranuclear inclusions in striatal and cortical neurons in R6/2 transgenic mice. J. Comp. Neurol. 449, 241–269. https://doi.org/10.1002/cne.10295.
Menalled, L.B., Kudwa, A.E., Oakeshott, S., Farrar, A., Paterson, N., Filippov, I., Miller, S., et al., 2014. Genetic deletion of transglutaminase 2 does not rescue the phenotypic deficits observed in R6/2 and zQ175 mouse models of Huntington's disease. PLoS One 9, e99520. https://doi.org/10.1371/journal.pone.0099520.
Mochel, F., Duteil, S., Marelli, C., Jauffret, C., Barles, A., Holm, J., Sweetman, L., Benoist, J.F., Rabier, D., Carlier, P.G., Durr, A., 2010. Dietary anaplerotic therapy improves peripheral tissue energy metabolism in patients with Huntington's disease. Eur. J. Hum. Genet. 18, 1057–1060. https://doi.org/10.1038/ejhg.2010.72.
Morton, A.J., Glynn, D., Leavens, W., Zheng, Z., Faull, R.L., Skepper, J.N., Wight, J.M., 2009. Paradoxical delay in the onset of disease caused by super-long CAG repeat expansions in R6/2 mice. Neurobiol. Dis. 33, 331–341. https://doi.org/10.1016/j.nbd.2008.11.015.
Norgren, N., Rosengren, L., Stigbrand, T., 2003. Elevated neurofilament levels in neurological diseases. Brain Res. 987, 25–31. https://doi.org/10.1016/S0006-8993(03)03219-0.
Novak, M.J., Tabrizi, S.J., 2010. Huntington's disease. Bmj 340, c3109. https://doi.org/10.1136/bmj.c3109.
Oldreive, C.E., Harvey, J., Doherty, G.H., 2008. Neurotrophic effects of leptin on cerebellar Purkinje but not granule neurons in vitro. Neurosci. Lett. 438, 17–21. https://doi.org/10.1016/j.neulet.2008.04.045.
Pagliassotti, M.J., Kim, P.Y., Estrada, A.L., Stewart, C.M., Gentile, C.L., 2016. Endoplasmic reticulum stress in obesity and obesity-related disorders: an expanded view. Metab. Clin. Exp. 65, 1238–1246. https://doi.org/10.1016/j.metabol.2016.05.002.
Panchal, S.K., Brown, L., 2011. Rodent models for metabolic syndrome research. J. Biomed. Biotechnol. 2011, 351982. https://doi.org/10.1155/2011/351982.
Park, J.H., Hong, Y.H., Kim, H.J., Kim, S.M., Kim, M.J., Park, K.S., Sung, J.J., Lee, K.W., 2007. Pyruvate slows disease progression in a G93A SOD1 mutant transgenic mouse model. Neurosci. Lett. 413, 265–269. https://doi.org/10.1016/j.neulet.2006.11.058.
Passani, L.A., Bedford, M.T., Faber, P.W., McGinnis, K.M., Sharp, A.H., Gusella, J.F., Vonsattel, J.P., MacDonald, M.E., 2000. Huntingtin's WW domain partners in Huntington's disease post-mortem brain fulfill genetic criteria for direct involvement in Huntington's disease pathogenesis. Hum. Mol. Genet. 9, 2175–2182. https://doi.org/10.1093/hmg/9.14.2175.
Paulsen, J.S., Miller, A.C., Hayes, T., Shaw, E., 2017. Cognitive and behavioral changes in Huntington disease before diagnosis. Handb. Clin. Neurol. 144, 69–91. https://doi.org/10.1016/B978-0- 12-801893-4.00006-7.
Paumier, K.L., Sukoff Rizzo, S.J., Berger, Z., Chen, Y., Gonzales, C., Kaftan, E., Li, L., Lotarski, S., Monaghan, M., Shen, W., Stolyar, P., Vasilyev, D., Zaleska, M., Hirst, W.D., Dunlop, J., 2013. Behavioral characterization of A53T mice reveals early and late stage deficits related to Parkinson's disease. PLoS One 8, e70274. https://doi.org/10.1371/journal.pone.0070274.
Petersen, A., Bjorkqvist, M., 2006. Hypothalamic-endocrine aspects in Huntington's disease. Eur. J. Neurosci. 24, 961–967. https://doi.org/10.1111/j.1460- 9568.2006.04985.x.
Petersen, A., Gabery, S., 2012. Hypothalamic and limbic system changes in Huntington's disease. J. Huntington's Dis. 1, 5–16. https://doi.org/10.3233/JHD-2012-120006.
Poudel, G.R., Stout, J.C., Dominguez, D.J., Churchyard, A., Chua, P., Egan, G.F., Georgiou-Karistianis, N., 2015. Longitudinal change in white matter microstructure in Huntington's disease: the IMAGE-HD study. Neurobiol. Dis. 74, 406–412. https://doi.org/10.1016/j.nbd.2014.12.009.
Rohrer, J.D., Woollacott, I.O., Dick, K.M., Brotherhood, E., Gordon, E., Fellows, A., Toombs, J., Druyeh, R., Cardoso, M.J., Ourselin, S., Nicholas, J.M., Norgren, N., Mead, S., Andreasson, U., Blennow, K., Schott, J.M., Fox, N.C., Warren, J.D., Zetterberg, H., 2016. Serum neurofilament light chain protein is a measure of disease intensity in frontotemporal dementia. Neurology 87, 1329–1336. https://doi.org/10.1212/WNL.0000000000003154.
Rosas, H.D., Lee, S.Y., Bender, A.C., Zaleta, A.K., Vangel, M., Yu, P., Fischl, B., Pappu, V., Onorato, C., Cha, J.H., Salat, D.H., Hersch, S.M., 2010. Altered white matter microstructure in the corpus callosum in Huntington's disease: implications for cortical "disconnection". NeuroImage 49, 2995–3004. https://doi.org/10.1016/j.neuroimage.2009.10.015.
Ross, C.A., Tabrizi, S.J., 2011. Huntington's disease: from molecular pathogenesis to clinical treatment. Lancet Neurol. 10, 83–98. https://doi.org/10.1016/S1474-4422(10)70245-3.
Rousset, S., Alves-Guerra, M.C., Mozo, J., Miroux, B., Cassard-Doulcier, A.M., Bouillaud, F., Ricquier, D., 2004. The biology of mitochondrial uncoupling proteins. Diabetes 53 (Suppl. 1), S130–S135. https://doi.org/10.2337/diabetes.53.2007.S130.
Sathasivam, K., Hobbs, C., Turmaine, M., Mangiarini, L., Mahal, A., Bertaux, F., Wanker, E.E., Doherty, P., Davies, S.W., Bates, G.P., 1999. Formation of polyglutamine inclusions in non-CNS tissue. Hum. Mol. Genet. 8, 813–822. https://doi.org/10.1093/hmg/8.5.813.
Sena, A., Sarlièvе, L.L., Rebel, G., 1985. Brain myelin of genetically obese mice. J. Neurol. Sci. 68, 233–243. https://doi.org/10.1016/0022-510X(85)90104-2.
She, P., Zhang, Z., Marchionini, D., Diaz, W.C., Jetton, T.J., Kimball, S.R., Vary, T.C., Lang, C.H., Lynch, C.J., 2011. Molecular characterization of skeletal muscle atrophy in the R6/2 mouse model of Huntington's disease. Am. J. Phys. Endocrinol. Metab. 301, E49–E61. https://doi.org/10.1152/ajpendo.00630.2010.
Sjögren, M., Duarte, A.I., McCourt, A.C., Shcherbina, L., Wierup, N., Björkqvist, M., 2017. Ghrelin rescues skeletal muscle catabolic profile in the R6/2 mouse model of Huntington's disease. Sci. Rep. 7, 13896. https://doi.org/10.1038/s41598-017-13713-5.
Soylu-Kucharz, R., Sandelius, Å., Sjögren, M., Blennow, K., Wild, E.J., Zetterberg, H., Björkqvist, M., 2017. Neurofilament light protein in CSF and blood is associated with neurodegeneration and disease severity in Huntington's disease R6/2 mice. Sci. Rep. 7, 14114. https://doi.org/10.1038/s41598-017-14179-1.
Strand, A.D., Aragaki, A.K., Shaw, D., Bird, T., Holton, J., Turner, C., Tapscott, S.J., Tabrizi, S.J., Schapira, A.H., Kooperberg, C., Olson, J.M., 2005. Gene expression in Huntington's disease skeletal muscle: a potential biomarker. Hum. Mol. Genet. 14, 1863–1876. https://doi.org/10.1093/hmg/ddi192.
Szczypka, M.S., Rainey, M.A., Palmiter, R.D., 2000. Dopamine is required for hyperphagia in Lep(ob/ob) mice. Nat. Genet. 25, 102–104. https://doi.org/10.1038/75484.
Udagawa, J., Hatta, T., Hashimoto, R., Otani, H., 2007. Roles of leptin in prenatal and perinatal brain development. Congenit Anom (Kyoto) 47, 77–83. https://doi.org/10.1111/j.1741- 4520.2007.00150.x.
Valenza, M., Carroll, J.B., Leoni, V., Bertram, L.N., Björkhem, I., Singaraja, R.R., Di Donato, S., et al., 2007. Cholesterol biosynthesis pathway is disturbed in YAC128 mice and is modulated by huntingtin mutation. Hum. Mol. Genet. 16, 2187–2198. https://doi.org/10.1093/hmg/ddm170.
Vandoorne, T., De Bock, K., Van Den Bosch, L., 2018. Energy metabolism in ALS: an underappreciated opportunity? Acta Neuropathol. 135, 489–509. https://doi.org/10.1007/s00401-018-1835-x.
Verdile, G., Fuller, S.J., Martins, R.N., 2015. The role of type 2 diabetes in neurodegeneration. Neurobiol. Dis. 84, 22–38. https://doi.org/10.1016/j.nbd.2015.04.008.
Vonsattel, J.P., 2008. Huntington disease models and human neuropathology: similarities and differences. Acta Neuropathol. 115, 55–69. https://doi.org/10.1007/s00401-007-0306-6.
Walker, F.O., 2007. Huntington's disease. Lancet 369, 218–228. https://doi.org/10.1016/S0140-6736(07)60111-1.
Wallace, T.M., Levy, J.C., Matthews, D.R., 2004. Use and abuse of HOMA modeling. Diabetes Care 6, 1487–1495. https://doi.org/10.2337/diacare.27.6.1487.
Zhang, J., Gregory, S., Scahill, R.I., Durr, A., Thomas, D.L., Lehericy, S., Rees, G., Tabrizi, S.J., Zhang, H., TrackOn HDi, 2018. In vivo characterization of white matter pathology in premanifest huntington's disease. Ann. Neurol. 84, 497–504. https://doi.org/10.1002/ana.2530.